1

Fundamentals of Capillarity

1.1 Abstract

In this first chapter, the fundamentals of capillarity are presented. We follow a conventional approach [1], first presenting surface tension of an interface, which is the fundamental notion in capillarity theory; this notion leads naturally to that of wetting, then to Laplace's law, and to the introduction of Young contact angles and capillary forces. Next, different applications of capillary forces are shown, and the problem of the measurement of surface tensions is presented.

1.2 Interfaces and Surface Tension

1.2.1 The Notion of Interface

Mathematically speaking, an interface is the geometrical surface that delimits two fluid domains. This definition implies that an interface has no thickness and is smooth (i.e. has no roughness). As practical as it is, this definition is in reality a schematic concept. The reality is more complex, the boundary between two immiscible liquids is somewhat blurred and the separation of the two fluids (water/air, water/oil, etc.) depends on molecular interactions between the molecules of each fluid [2] and on Brownian diffusion (thermal agitation). A microscopic view of the interface between two fluids looks more like the scheme of figure 1.1. However,

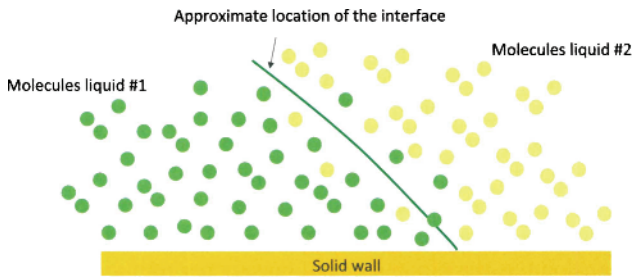

Figure 1.1 Schematic view of an interface at the molecular size.

in engineering applications, it is the macroscopic behavior of the interface that is the focus of attention, and the mathematical concept regains its utility. At a macroscopic size, the picture of figure 1.1 can be replaced by that of figure 1.2, where the interface is a mathematical surface without thickness and the contact angle θ is uniquely defined by the tangent to the surface at the contact line.

In a condensed state, molecules attract each other. Molecules located in the bulk of a liquid have interactions with neighboring molecules on all sides; these interactions are mostly van der Waals attractive interactions for organic liquids and hydrogen bonds for polar liquids like water [2]. On the other hand, molecules at an interface have interactions in a half space with molecules of the same liquid, and in the other half space interactions with molecules of the other fluid or gas (figure 1.3).

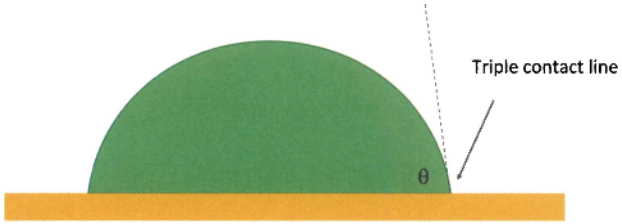

Figure 1.2 Macroscopic view of the interface of a drop.

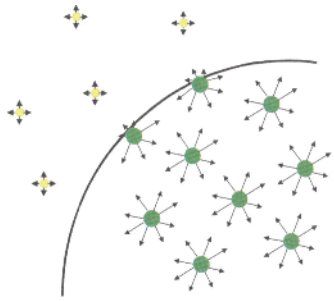

Figure 1.3 Simplified scheme of molecules near an air/water interface. In the bulk, molecules have interaction forces with all the neighboring molecules. At the interface, half of the interactions have disappeared.

Consider an interface between a liquid and a gas. In the bulk of the liquid, a molecule is in contact with 4 to 12 other molecules depending on the liquid (4 for water and 12 for simple molecules); at the interface this number is divided by two. Of course, a molecule is also in contact with gas molecules, but, due to the low densities of gases, there are fewer interactions and less attraction than on the liquid side. The result is that there is locally a dissymmetry in the interactions, which results in an excess of surface energy. At the macroscopic scale, a physical quantity called "surface tension" has been introduced in order to take into account this molecular effect. The surface tension has the dimensions of energy per unit area, and in the International System it is expressed in J/m^2 or N/m (sometimes, it is more practical to use mN/m as a unit for surface tension). An estimate of the surface tension can be found by considering the molecules' cohesive energy. If U is the total cohesive energy per molecule, a rough estimate of the energy

excess of a molecule at the interface is $U/2$. Surface tension is a direct measure of this energy excess, and if δ is a characteristic molecular dimension and δ^2 the associated molecular surface area, then the surface tension is approximately

$$\gamma \approx \frac{U}{\delta^2}. \tag{1.1}$$

This relation shows that surface tension is important for liquids with large cohesive energy and small molecular dimension. This is why mercury has a large surface tension whereas oil and organic liquids have small surface tensions. Another consequence of this analysis is the fact that a fluid system will always act to minimize surface area: the larger the surface area, the larger the number of molecules at the interface and the larger the cohesive energy imbalance. Molecules at the interface always look for other molecules to equilibrate their interactions. As a result, in the absence of other forces, interfaces tend to adopt a flat profile, and when it is not possible due to boundary constraints or volume constraints, they take a rounded shape, often that of a sphere. Another consequence is that it is energetically costly to expand or create an interface: we will come back on this problem in Chapter 10 when dividing a droplet into two "daughter" droplets by electrowetting actuation. The same reasoning applies to the interface between two liquids, except that the interactions with the other liquid will usually be more attractive than a gas and the resulting dissymmetry will be less. For example, the contact energy (surface tension) between water and air is 72 mN/m, whereas it is only 50 mN/m between water and oil (table 1.1). Interfacial tension between two liquids may be zero: fluids with zero interfacial tension are said to be miscible. For example, there is no surface tension between fresh and salt water: salt molecules will diffuse freely across a boundary between fresh and saltwater.

The same principle applies for a liquid at the contact of a solid. The interface is just the solid surface at the contact of the liquid. Molecules in the liquid are attracted towards the interface by van der Waals forces. If the attractions to the solid are strong, the liquid-solid interface has negative surface energy, and the solid is said to be wetting or hydrophilic (or lyophilic for non-water liquids, but we will use the term hydrophilic for all liquids). If the attractions are weak, the interface energy is positive, and the solid is nonwetting or hydrophobic (or lyophobic).

Usually surface tension is denoted by the Greek letter γ, with subscripts referring to the two components on each side of the interface, for example γ_{LG} at a Liquid/Gas interface. Sometimes, if the contact is with air, or if no confusion can be made, the subscripts can be omitted. It is frequent to speak of "surface tension" for a liquid in contact with a gas, and "interfacial tension" for a liquid in contact with another liquid. According to the definition of surface tension, for a homogeneous interface (same molecules at the interface all along the interface), the total energy of a surface is

$$E = \gamma S, \tag{1.2}$$

where S is the interfacial surface area.

In the literature or on the Internet there exist tables for surface tension values [3,4]. Typical values of surface tensions are given in table 1.1. Note that surface tension increases as the intermolecular attraction increases and the molecular size decreases. For most oils, the value of the surface tension is in the range $\gamma \approx 20 - 30$ mN/m, while for water, $\gamma \approx 70$ mN/m. The highest surface tensions are for liquid metals; for example, liquid mercury has a surface tension $\gamma \approx 500$ mN/m.

Table 1.1 Values of surface tension of different liquids in contact with air at a temperature of 20 °C (middle column, mN/m) and thermal coefficient α (right column, mN/m/°C).

liquid	γ_0	α
Acetone	25.2	−0.112
Benzene	28.9	−0.129
Benzylbenzoate	45.95	−0.107
Bromoform	41.5	−0.131
Chloroform	27.5	−0.1295
Cyclohexane	24.95	−0.121
Cyclohexanol	34.4	−0.097
Decalin	31.5	−0.103
Dichloroethane	33.3	−0.143
Dichloromethane	26.5	−0.128
Ethanol	22.1	−0.0832
Ethylbenzene	29.2	−0.109
Ethylene-Glycol	47.7	−0.089
Isopropanol	23.0	−0.079
Iodobenzene	39.7	−0.112
Glycerol	64.0	−0.060
Mercury	425.4	−0.205
Methanol	22.7	−0.077
Nitrobenzene	43.9	−0.118
Perfluorooctane	14.0	−0.090
Polyethylen-glycol	43.5	−0.117
PDMS	19.0	−0.036
Pyrrol	36.0	−0.110
Toluene	28.4	−0.119
Water	72.8	−0.1514

1.2.2 The Effect of Temperature on Surface Tension

The value of the surface tension depends on the temperature. The first empirical equation for the surface tension dependence on temperature was given by Eötvös in 1886 [5]. Observing that the surface tension goes to zero when the temperature tends to the critical temperature T_C, Eötvös proposed the semi-empirical relation

$$\gamma = \left(\frac{1}{v_L}\right)^{\frac{2}{3}} (T - T_C), \tag{1.3}$$

where v_L is the molar volume. Katayama (1915) and later Guggenheim (1945) [6] have improved Eötvs's relation to obtain

$$\gamma = \gamma^* \left(1 - \frac{T}{T_C}\right)^n, \tag{1.4}$$

where γ^* is a constant for each liquid and n is an empirical factor, whose value is 11/9 for organic liquids. Equation (1.4) produces very good results for organic liquids. If temperature variation is not very important, and taking into account that the exponent n is close to 1, a good approximation of the Guggenheim-Katayama formula is the linear approximation

$$\gamma = \gamma^*(1 + \alpha T). \tag{1.5}$$

It is often easier and more practical to use a measured reference value (γ_0, T_0) and consider a linear change of the surface tension with the temperature,

$$\gamma = \gamma_0(1 + \beta(T - T_0)). \tag{1.6}$$

Comparison between (1.4) and (1.6) for $\gamma = 0$ at $T = T_C$ requires

$$\beta = -\frac{1}{T_C - T_0}. \tag{1.7}$$

Relations (1.5) and (1.6) are shown in figure 1.4. The value of the reference surface tension γ_0 is linked to γ^* by the relation

$$\gamma^* = \gamma_0 \frac{T_C - T_0}{T_0}. \tag{1.8}$$

Typical values of surface tensions and their temperature coefficients α are given in table 1.1.

The coefficient α being always negative, the value of the surface tension decreases with temperature. This property is at the origin of a phenomenon which is called either Marangoni convection or thermocapillary instability (figure 1.5). If an interface is locally heated by any heat source (such as radiation, convection or conduction), the surface tension is reduced on the heated area according to equations (1.5) or (1.6) . A gradient of surface tension is then induced at the interface between the cooler interface and the warmer interface. We will show in section 1.3.7 that surface tensions can be viewed as forces; as a consequence, there is an imbalance of tangential forces on the interface, creating a fluid motion starting from the warm region (smaller value of the surface tension) towards the cooler region (larger value of the surface tension). This surface motion propagates to the bulk under the influence of viscosity. If the temperature source is temporary, the motion of the fluid tends to homogenize the temperature and the motion gradually stops. If a difference of temperature is maintained on the interface,

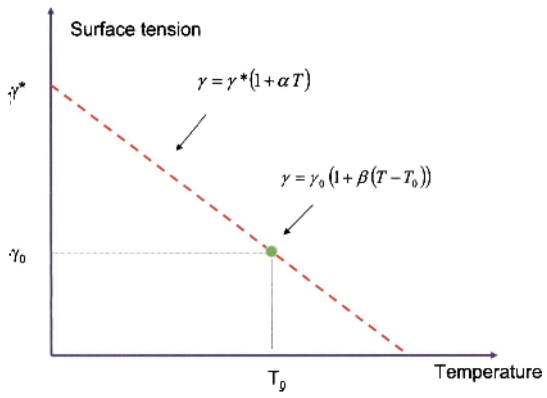

Figure 1.4 Representation of the relations (1.5) and (1.6).

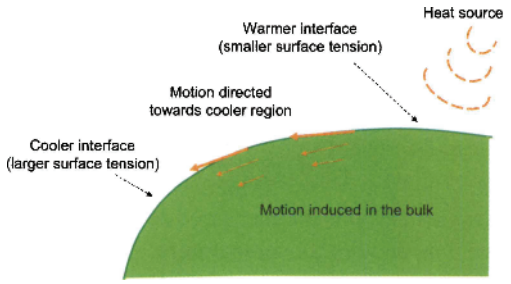

Figure 1.5 Sketch of interface motion induced by a thermal gradient between two regions of the surface. The motion of the interface propagates into the bulk under the action of viscous forces.

the motion of the fluid is permanent; this is the case of a film of liquid spread on a warm solid. Depending on the contrast of temperature between the solid surface and the liquid surface, the motion of the liquid in the film has the morphology of convective rolls, hexagons or squares. Figure 1.6 shows hexagonal patterns of Marangoni convection in a film of liquid heated from below [7]. The white streamlines in the left image show the trajectories of the liquid molecules.

1.2.3 The Effect of Surfactants

"Surfactant" is the short term for "surface active agent". Surfactants are long molecules characterized by a hydrophilic head and a hydrophobic tail, and are for this reason called amphiphilic molecules. Very often surfactants are added to biological samples in order to prevent the formation of aggregates and to prevent target molecules from adhering to the solid walls of the microsystem (remember that microsystems have extremely large ratios between the wall areas and the liquid volumes). Surfactants diffuse in the liquid, and when reaching the interface they are captured because their amphiphilic nature prevents them from escaping easily from the interface. As a consequence, they gather on the interface, as is sketched in figure 1.7, lowering the surface tension of the liquid.

As the concentration of surfactants increases, the surface concentration increases also.

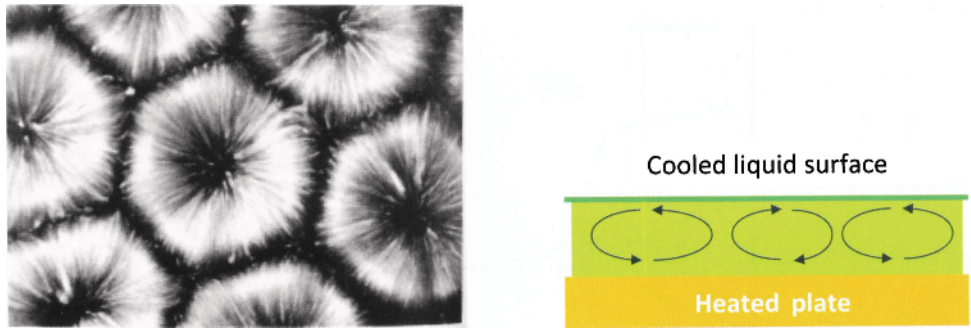

Figure 1.6 Marangoni convection, due to thermocapillary instabilities, makes hexagonal patterns in a thin film of liquid. Reprinted with permission from [7], ©AIP 2005.

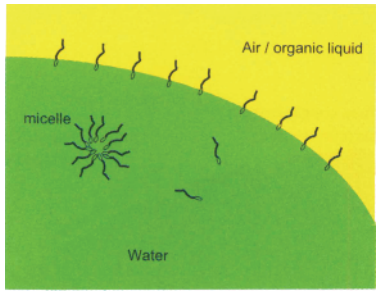

Figure 1.7 Schematic view of surfactants in a liquid drop.

Above a critical value of the concentration, called CMC for Critical Micelle Concentration, the interface is saturated with surfactants, and surfactant molecules in the bulk of the fluid group together to form micelles. The evolution of the value of the surface tension as a function of the concentration in surfactants is shown in figure 1.8. At very low concentration, the slope is nearly linear; when the concentration approaches the CMC, the value of the surface tension drops sharply; above CMC, the value of the surface tension is nearly constant [8]. For example, pure water has a surface tension 72 mN/m, and water with Tween 80 at a concentration above the CMC has a surface tension of only 30 mN/m.

In the limit of small surfactant concentration ($c \ll$ CMC), the surface tension can be expressed as a linear function of the concentration

$$\gamma = \gamma_0(1 + \beta(c - c_0)). \tag{1.9}$$

Equation (1.9) is similar to equation (1.6) (different β, of course). We have seen how a temperature gradient results in a gradient of surface tension leading to Marangoni type of convection. Similarly, a concentration gradient results in a gradient of surface tension, and consequently to a Marangoni convection, as in figure 1.9. Note that the direction of the motion is always towards the largest value of surface tension. Spreading of surfactant molecules on an interface can be easily seen experimentally: an instructive example is that of a thin paper boat with a cavity at the rear (figure 1.10). When the boat is placed gently on the surface of water, it rests on the surface of water suspended by surface tension forces. Upon putting a drop of soap solution/detergent in the notch, boat accelerates rapidly. Soap molecules try to spread over the surface of water.

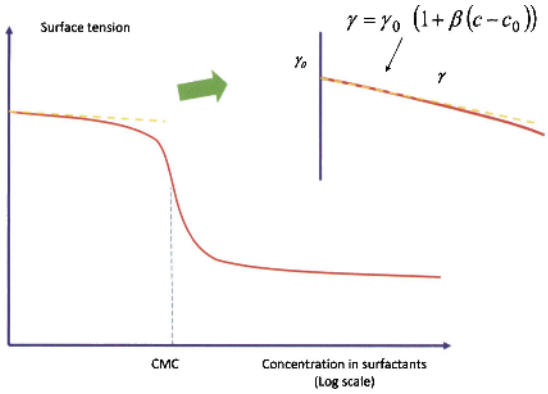

Figure 1.8 Evolution of the value of the surface tension as a function of the surfactant concentration.

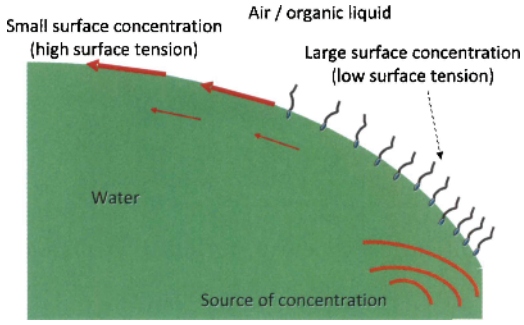

Figure 1.9 Schematic Marangoni convection induced by a gradient of concentration.

Since they are confined in the cavity of boat with only way out, they reduce the surface tension only at the rear, creating a net force which drives the boat forward.

1.2.4 Surface Tension of a Fluid Containing Particles

Pure fluids are seldom used, especially in biotechnology. Very often micro- and nano-particles are present and transported by the fluid or they are voluntarily added to the fluid. Depending on their concentration and nature, the presence of micro- or nano-particles in the fluid might modify considerably the value of the surface tension (figure 1.11). At the same time, the presence of micro-particles reduces the contact angle. The notion of contact angle will be discussed later on in this chapter.

This decrease in surface tension depends on the concentration, size and nature of the micro-particles; at the molecular scale, it is linked to the interactions between particles and liquid on one hand, and between particles themselves on the other hand [10].

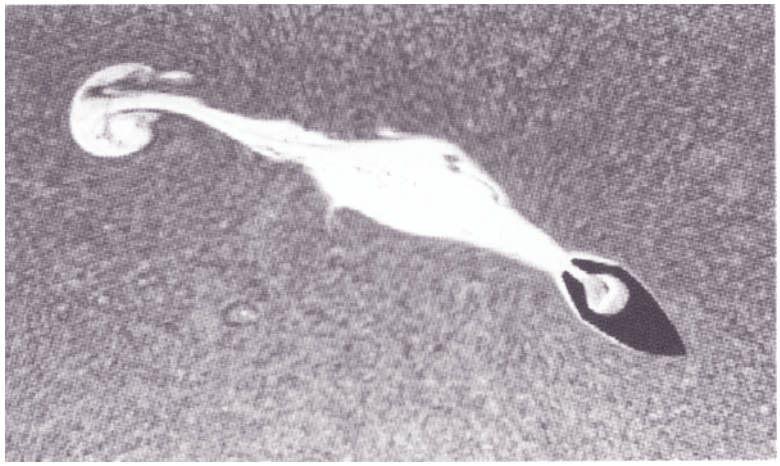

Figure 1.10 Soap boat: a floating body contains a small volume of soap. At first, the soap exits the rear of the boat under Marangoni stress. Hence a low surface tension region is created behind the boat, whereas the unsoaped region in front of the boat has a larger surface tension. This difference of surface tension pulls the boat forward (courtesy MIT: http://web.mit.edu/1.63/www/Lec-notes/Surfacetension/Lecture4.pdf [9]).

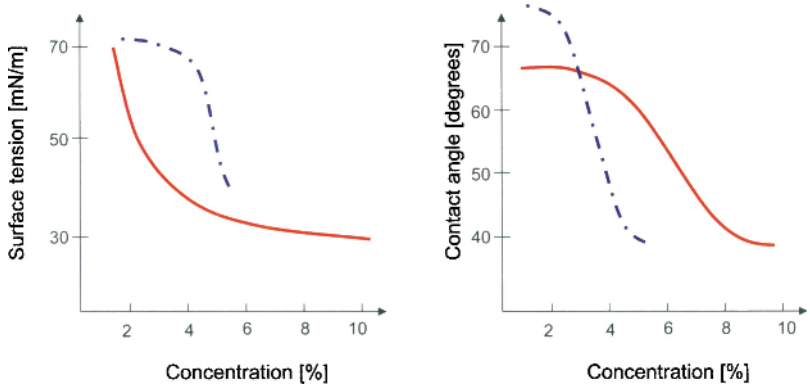

Figure 1.11 Left, surface tension of two different kinds of 10 μm polystyrene particles; right, corresponding equilibrium contact angles.

1.3 Laplace's Law and Applications

Laplace's law is fundamental when dealing with interfaces and micro-drops. It relates the pressure inside a droplet to the curvature of the droplet. This section first describes the mathematical notion of the curvature of a surface, then how it relates to surface tension and pressure, followed by a number of applications.

1.3.1 Curvature and Radius of Curvature

For a planar curve the radius of curvature at a point is the radius R of the osculating circle at that point – the circle which is the closest to the curve at the contact point (figure 1.12). The curvature of the curve at the point is defined by

$$\kappa = \frac{1}{R}. \tag{1.10}$$

Note that the curvature as well as the curvature radius are signed quantities. Curvature radius

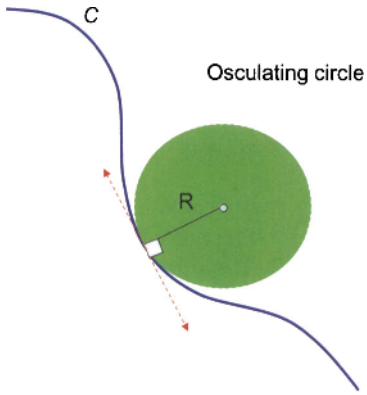

Figure 1.12 Radius of curvature and osculating circle.

can be positive or negative depending on the orientation (convex or concave) of the curve. The curvature may be equivalently defined as the rate of change of the direction angle of the tangent vector with respect to arc length. In the case of a parametric curve $c(t) = (x(t), y(t))$, the curvature is given by the relation [11]

$$\kappa = \frac{\dot{x}\ddot{y} - \ddot{x}\dot{y}}{(\dot{x}^2 + \dot{y}^2)^{\frac{3}{2}}}, \tag{1.11}$$

where the dot denotes a differentiation with respect to t. For a plane curve given implicitly as $f(x,y) = 0$, the curvature is

$$\kappa = \Delta \cdot \left(\frac{\nabla f}{\|\nabla f\|} \right), \tag{1.12}$$

that is, the divergence of the direction of the gradient of f. And for an explicit function $y = f(x)$, the curvature is defined by

$$\kappa = \frac{\frac{d^2y}{dx^2}}{(1 + (\frac{dy}{dx})^2)^{\frac{3}{2}}}. \tag{1.13}$$

The situation is more complex for a surface. Any plane containing the vector normal to the surface intersects the surface along a curve. Each of these curves has its own curvature, called a sectional curvature, signed with respect to the orientation of the surface. The mean curvature of

the surface is defined using the principal (maximum and minimum) curvatures κ_1 and κ_2 (figure 1.13) in the whole set of curvatures:

$$H = \frac{1}{2}(\kappa_1 + \kappa_2). \tag{1.14}$$

It can be shown that the principal curvatures κ_1 and κ_1 are located in two perpendicular planes. In fact, it turns out that the sum of the sectional curvatures in any two perpendicular directions is the same. Introducing the curvature radii in (1.14) leads to

$$H = \frac{1}{2}(\kappa_1 + \kappa_2) = \frac{1}{2}\left(\frac{1}{R_1} + \frac{1}{R_2}\right). \tag{1.15}$$

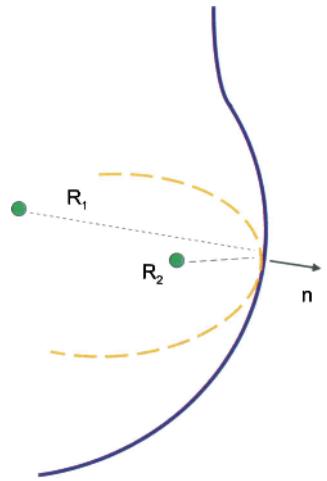

Figure 1.13 Schematic view of the curvature radii of a surface. The dashed and solid curves are the intersections of the surface with two planes perpendicular to the surface and each other.

For a sphere of radius R, the two curvatures are equal to $1/R$ and the mean curvature is $H = 1/R$. For a cylinder of base radius R, the maximum curvature is R and the minimum curvature zero, hence $H = 1/(2R)$. For a plane, the two curvatures are zero and so $H = 0$: a plane has no curvature. At a saddle point of a surface (figure 1.14), one of the curvature radii is positive because it corresponds to a convex arc, whereas the other one is negative, because it corresponds to a concave arc. If $|R_1| = |R_2|$ then the mean curvature H is zero,

$$H = \frac{1}{2}\left(\frac{1}{R_1} + \frac{1}{R_2}\right) = \frac{1}{2}\left(\frac{1}{|R_1|} - \frac{1}{|R_2|}\right) = 0. \tag{1.16}$$

1.3.2 Derivation of Laplace's Law

Suppose a spherical droplet of liquid surrounded by a fluid. Let us calculate the work necessary to increase its volume from the radius R to the radius $R + dR$ (figure 1.15). The part of the work due to the internal volume increase is

$$\delta W_i = -P_0 dV_0, \tag{1.17}$$

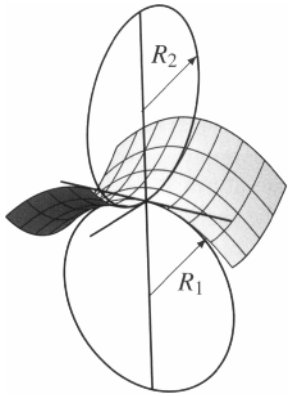

Figure 1.14 The mean curvature at a point is zero if it is a saddle point with equal but opposite sectional curvatures, $|R_1| = |R_2|$.

where dV_0 is the increase of the volume of the droplet,

$$dV_0 = 4\pi R^2 dR. \tag{1.18}$$

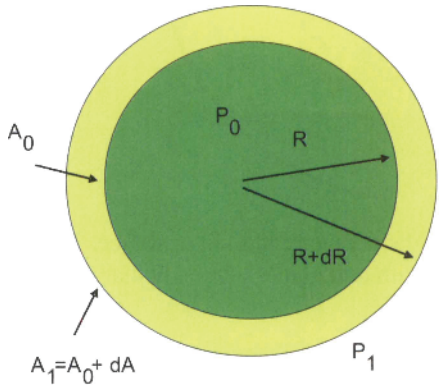

Figure 1.15 Schematic of a liquid drop immersed in a fluid; initially, the droplet radius is R and its surface area A_0. An increase of its radius by a quantity dR corresponds to the new surface area A_1 and the pressure P_1.

The work to pull out the external fluid is

$$\delta W_e = -P_1 dV_1, \tag{1.19}$$

where dV_1 is the decrease of the external volume, equal to $-dV_0$. The work corresponding to the increase of interfacial area is

$$dW_S = \gamma dA, \tag{1.20}$$

where dA is the increase of the surface area. The mechanical equilibrium condition is then

$$\delta W = \delta W_i + \delta W_e + \delta W_s = 0. \tag{1.21}$$

Substituting the values of the work found previously, it follows that

$$\delta P = P_1 - P_0 = 2\frac{\gamma}{R}. \tag{1.22}$$

Equation (1.22) is the Laplace equation for a sphere. The reasoning we have done to obtain equation (1.22) can be generalized,

$$\delta P = \gamma \frac{dA}{dV}. \tag{1.23}$$

For simplicity, we have derived Laplace's equation for the case of a sphere, but we can use (1.23) for an interface locally defined by two (principal) radii of curvature R_1 and R_2; the result would have been then

$$\delta P = \gamma \left(\frac{1}{R_1} + \frac{1}{R_2} \right). \tag{1.24}$$

For a cylindrical interface, as sketched in figure 1.16, one of the two radii of curvature is infinite, and Laplace's equation reduces to

$$\delta P = \frac{\gamma}{R}. \tag{1.25}$$

Equation (1.24) is called Laplace's law. Keep in mind that it is closely linked to the minim-

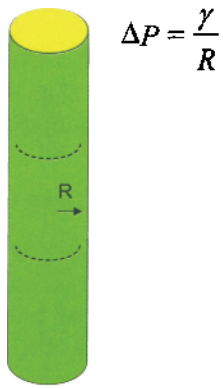

Figure 1.16 Laplace's law for a cylindrical interface.

ization of the energy. Laplace's law is fundamental when dealing with interfaces, micro-drops and in digital microfluidics. In the following section, we give some examples of application of Laplace's law.

1.3.3 Examples of Application of Laplace's Law

Amongst other things, Laplace's law explains many phenomena occurring during electrowetting actuation. We will talk about the use of Laplace's law for electrowetting in chapter 10. In this section, we present some applications of Laplace's law outside the electrowetting domain.

1.3.3.1 Pressure in a Bubble

The internal pressure in a bubble can be easily derived from the Laplace law (Fig. 1.17). If we assume that the thickness of the liquid layer is negligible in front of the bubble radius R, Laplace's law yields

$$\delta P = 2\gamma\left(\frac{1}{R_{ext}} + \frac{1}{R_{int}}\right) = \frac{4\gamma}{R}. \tag{1.26}$$

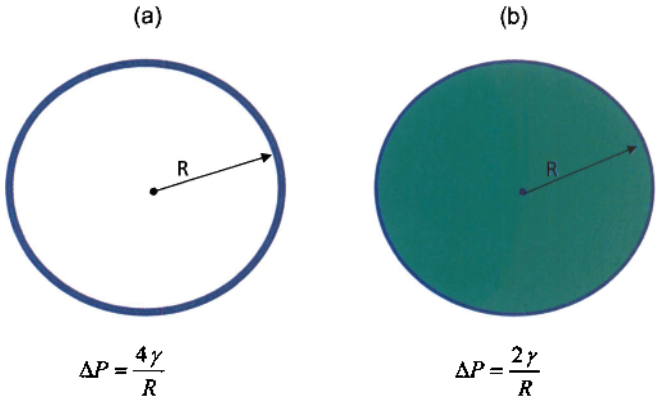

Figure 1.17 Comparison of the internal pressure in a bubble (a) and in a droplet of same radius (b).

The pressure in a bubble can be relatively high. For this reason, in children's kits for blowing bubbles, surfactants are added to the soap solution to facilitate bubble inflation.

1.3.3.2 Liquid Transfer From a Smaller Drop to a Bigger Drop

It has been observed that when two bubbles or droplets are connected together, there is a fluid flow from the small bubble/droplet to the larger one (figure 1.18). This is a direct application of Laplace's law: the pressure inside the small bubble/droplet is larger than that of the larger bubble/droplet, inducing a flow from towards the latter. This flow continues until the smaller bubble/droplet disappears to the profit of the larger one.

In biotechnology, this observation has been used to design microsystems where a microflow in a channel is set up by a difference of size of two droplets placed at both ends [12].

1.3.3.3 Precursor Film and Coarsening

At the beginning of this Chapter, we saw that the concept of an infinitely thin interface and a unique contact angle is a mathematical simplification of reality. When a partially wetting droplet is deposited on a flat solid surface, a very thin film of a few nanometers spreads before the contact line, and the contact between the liquid and the solid resembles the sketch of figure 1.19. The precursor film can be explained by thermodynamic considerations: because a jump between the chemical potential of the gas and of the solid is not physical, liquid molecules intercalate between the gas and the solid [13]. Molecules of the liquid progressively spread under the action of the "disjoining pressure" caused by the van der Waals interactions between

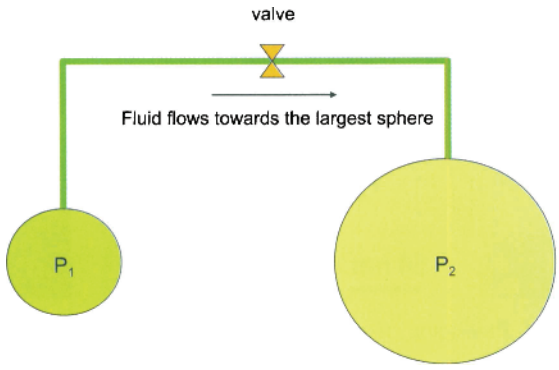

Figure 1.18 Fluid flow from the smaller bubble/droplet to the larger since the smaller bubble has higher curvature and thus higher pressure.

the liquid and solid molecules [14]. Precursor films exist for hydrophilic contact for static droplets as well as for dynamic wetting. Mechanisms of the advancing precursor film are still a subject of investigation [15].

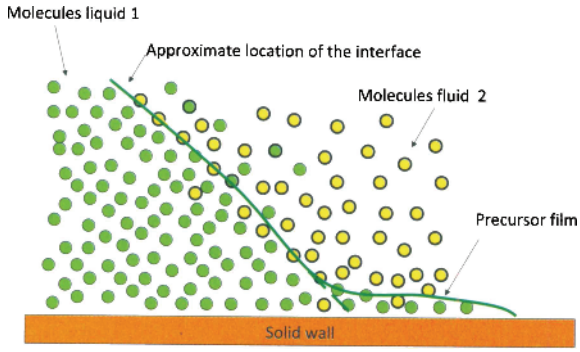

Figure 1.19 Interface with precursor film.

Such precursor films have been observed for different wetting situations, as shown in figure 1.20. Note the extreme thinness of the film in the photographs. When droplets of different size are deposited on a flat solid surface, if the droplets are sufficiently close to one another, it is observed that the smaller droplets disappear to the profit of the large droplets. This phenomenon is called "coarsening". Experimental evidence of coarsening is shown in figure 1.21.

The explanation of the phenomenon requires two steps: first, the existence of a precursor film (an extremely thin film on the solid surface spreading around each droplet) that links the droplets together; second, as in the previous example, the pressure is larger in a small droplet according to Laplace's law, and there is a liquid flow towards the largest droplet (figure 1.22). The precursor film is very thin, thus the flow rate between droplets is very small and mass transfer is extremely slow. Hence experimental conditions require that the droplets do not evaporate.

A numerical simulation of the transfer of liquid from the smaller droplet to the larger droplet can be easily performed using the Evolver as shown in figure 1.23. In the model, the precursor film is not modeled; the two initial droplets are simply united in the same logical volume.

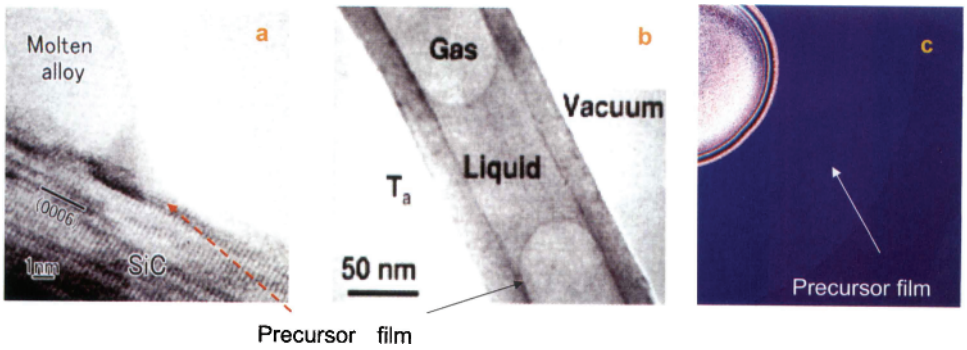

Figure 1.20 (a) Precursor film of spreading molten alloy (from [16], ©Elsevier, 2002); (b) precursor film of a liquid plug inside a carbon nanotube (from [17], ©AIP, 2005); (c) AFM scan on liquid crystal precursor film (from [18], courtesy Nanolane).

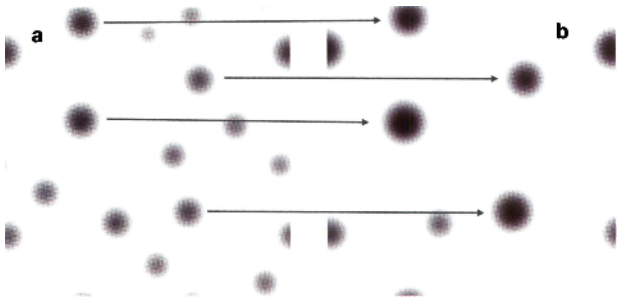

Figure 1.21 Experimental observation of coarsening: the number of droplets diminishes; only the largest droplets remain: (a) beginning of the observation, (b) increase in size of the large droplets and vanishing of the smaller droplets [19] (Courtesy Michael Bestehorn).

1.3.3.4 Pressure in Droplets Constrained Between Two Parallel Plates

When using Laplace's law, one should be careful of the orientation of the curvature. A convex surface has two positive radii of curvature. A "saddle" surface has one positive and one negative curvature radius. Take the example of a water droplet flattened between two horizontal plates (we will see in Chapter 3 that this situation is frequent in EWOD-based microsystems [20]). Suppose that the droplet is placed at the intersection of a hydrophobic band and a hydrophilic band. As a result, the droplet is squished by the hydrophobic band and elongated on the

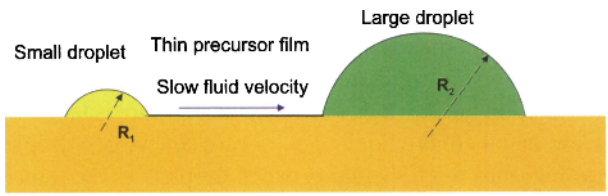

Figure 1.22 When two droplets are linked by a precursor film, a fluid flow is established from the smaller droplet to the larger droplet. The smaller droplet progressively disappears.

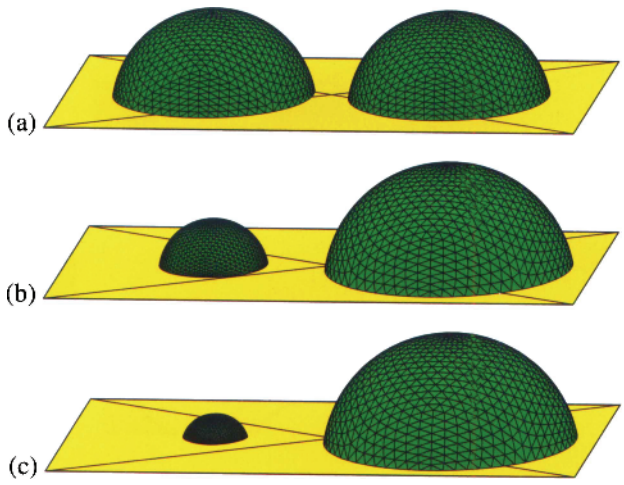

Figure 1.23 Evolver simulation of two droplets of slightly different volumes and supposedly in communication through the precursor film: liquid is transferred from the smaller droplet to the larger one.

hydrophilic band (figure 1.24). The pressure in the droplet is given by the Laplace law

$$P_{drop} - P_0 = \gamma\left(\frac{1}{R_1} + \frac{1}{R_2}\right) = \gamma\left(\frac{1}{R_3} + \frac{1}{R_4}\right), \tag{1.27}$$

where R_1, R_2, R_3 and R_4 are respectively the horizontal curvature radius in the hydrophilic region, the vertical curvature radius in the hydrophilic region, the horizontal curvature radius in the hydrophobic region, and the vertical curvature radius in the hydrophobic region. Taking into account the sign of the curvatures, we obtain

$$P_{drop} - P_0 = \gamma\left(\frac{1}{|R_1|} - \frac{1}{|R_2|}\right) = \gamma\left(\frac{1}{|R_4|} - \frac{1}{|R_3|}\right), \tag{1.28}$$

The pressure in the drop being larger than the exterior pressure is equivalent to satisfying either of the relations

$$|R_4| < |R_3| \tag{1.29}$$

or

$$|R_2| > |R_1|. \tag{1.30}$$

The vertical curvature radius R_4 in the hydrophobic region is smaller than the concave horizontal radius R_3 and the vertical curvature radius in the hydrophilic region R_2 is larger than the convex horizontal radius R_1. We shall see in Chapter 4 the use of a hydrophobic band to "cut" the droplet into two daughter droplets. For that to happen, the curvature radius R_3 must be sufficiently small, so that the two concave contact lines contact each other. The inequality (1.29) then produces a condition on the level of hydrophobicity required to obtain droplet division.

1.3.3.5 Zero Pressure Surfaces: Example of a Meniscus on a Rod

Laplace's law is often seen as a law determining a pressure difference on the two sides of the interface from the observation of curvature. But it is interesting to look at it the other

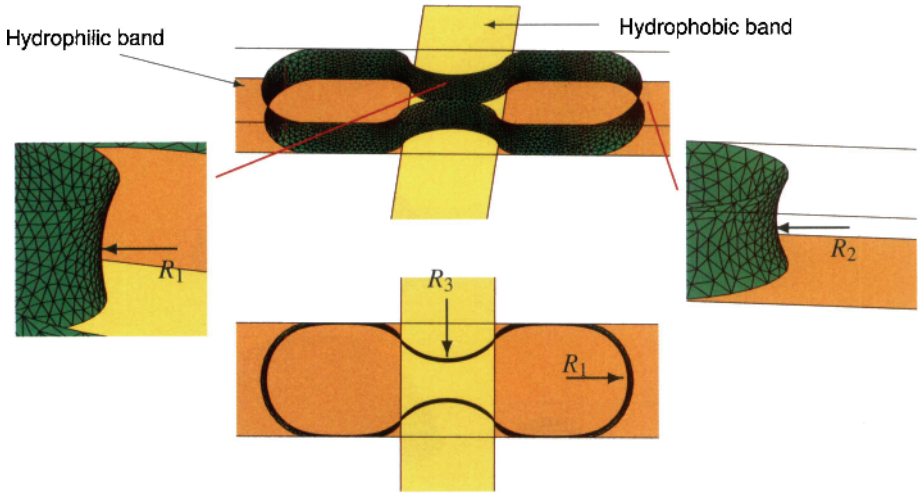

Figure 1.24 Sketch of a water droplet pinched by a hydrophobic surface. Case of a droplet constrained between two parallel planes (the upper plane has been dematerialized for visualization). Simulation performed with the Surface Evolver [21].

way: knowing the pressure difference, what conclusion may be reached on the curvature of the interface?

We consider an example in which the pressure difference is zero: this is the case of a cylindrical rod dipped in a wetting liquid. We suppose that the angle between the surface and the rod (contact angle) is $\theta = 0$. We shall develop the notion of contact angle in section 1.3.5. The liquid rises along the rod, deforming the free surface (figure 1.25). What is the shape of the surface? Laplace's law combined with the hydrostatic pressure yields

$$P_0 + \gamma\left(\frac{1}{R_1} + \frac{1}{R_2}\right) = P_0 - \rho g z, \tag{1.31}$$

where R_1 and R_2 are the two (signed) principal curvature radii. $R_1(z)$ is the (negative) curvature radius of the vertical profile at the elevation z, and $R_2(z)$ is the (positive) radius of the osculating circle perpendicular to the vertical (which is a tilted circle, not the circular horizontal cross-section). Assuming that the system is small enough that the gravity term can be neglected compared to the surface tension term, we are left with

$$\frac{1}{R_1} + \frac{1}{R_2} = 0. \tag{1.32}$$

This is the equation of a zero curvature surface, also called a minimal surface. The equation of the surface can be obtained by writing that the vertical projection of the surface tension force is constant [22]. Using the notations of figure 1.26, we find

$$2\pi r\gamma\cos\theta = 2\pi b\gamma. \tag{1.33}$$

Substituting the relation $\tan\theta = \frac{dr}{dz} = \dot{r}$, we are left with

$$\frac{r}{\sqrt{1+\dot{r}^2}} = b. \tag{1.34}$$

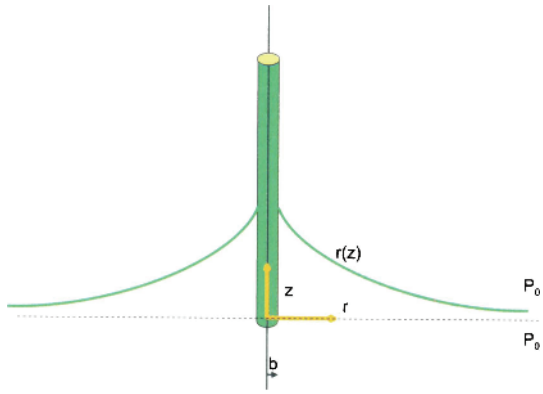

Figure 1.25 Sketch of rod dipped into a liquid (wetting case).

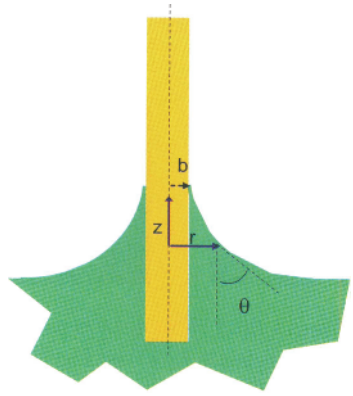

Figure 1.26 Vertical profile of liquid surface at the vicinity of a vertical rod.

Integration of (1.34) yields the equation of the vertical profile

$$r = b^* \cosh\left(\frac{z - h^*}{b^*}\right), \tag{1.35}$$

where b^* and h^* are constants depending on the contact angle with the vertical cylinder. In the case of a wetting contact ($\theta = 0$) the exact solution is

$$r = b \cosh\left(\frac{z - h_0}{b}\right), \tag{1.36}$$

where b is the wire radius and h_0 is the height of the interface along the wire. We note that equation (1.36) is the equation of a catenoid. Note that if the boundary of the surface is a circle at $z = 0$ of radius R_0, then z_0 goes to infinity as R_0 goes to infinity. This is not physical if any gravity is present; gravity flattens the surface so that the rise remains bounded for arbitrarily large R_0. We shall see in the following chapter that the expression

$$\kappa^{-1} = \sqrt{\frac{\gamma}{\rho g}} \tag{1.37}$$

is a characteristic height of capillarity in the presence of gravity, called the capillary length. Assuming that $b \ll h_0$, we can obtain an approximate value for the maximum height h_0 [22] by approximating the surface as a catenoid anchored on a ring of radius $R_0 = \kappa^{-1}$, which at $z = 0$ gives $\kappa^{-1} = b\cosh(-\frac{h_0}{b})$. Using $\cosh x \approx \frac{1}{2}\exp|x|$ for large $|x|$, we get

$$h_0 = b\ln\frac{2\kappa^{-1}}{b}. \tag{1.38}$$

Figure 1.27 shows the deformed surface obtained by a numerical simulation. Relation (1.38) shows that the elevation h_0 along the wire increases with the surface tension. At first sight, this may seem a paradox because the surface is pulled tighter when the surface tension increases. However, we show later in this Chapter that the capillary force exerted by the wire is proportional to the surface tension. The force pulling the surface is thus larger for high surface tension liquids.

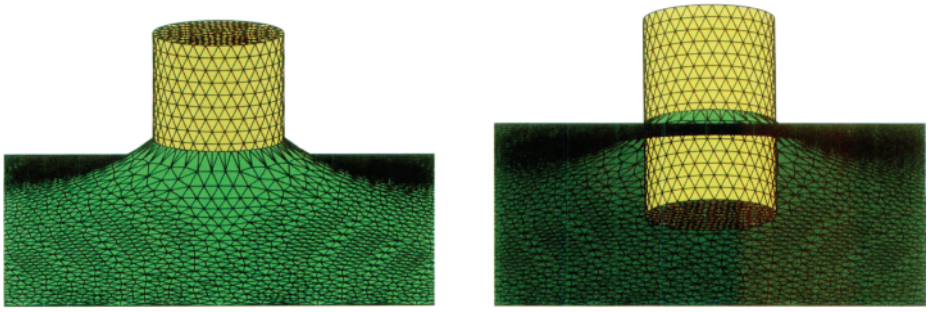

Figure 1.27 Vertical wire dipped into a fluid. The surface is deformed depending on the surface tension of the liquid and on the contact angle (Surface Evolver calculation). Left: view of the surface in the vicinity of the wire. Right: view from below showing the gain in elevation of the surface at the contact of the wire.

1.3.3.6 Self Motion of a Liquid Plug Between Two Non-Parallel Wetting Plates

It was first observed by Hauksbee [23] that a liquid plug between two non-parallel wetting plates moves towards the narrow gap. A sketch of the plug is shown in figure 1.28. Laplace's law furnishes a very clear explanation of this phenomenon. Suppose that figure 1.28 is a wedge (2D situation) and let us write Laplace's law for the left side interface

$$P_0 - P_1 = \frac{\gamma}{R_1}, \tag{1.39}$$

and for the right side interface

$$P_0 - P_2 = \frac{\gamma}{R_2}. \tag{1.40}$$

Subtraction of the two relations leads to

$$P_1 - P_2 = \gamma\left(\frac{1}{R_2} - \frac{1}{R_1}\right). \tag{1.41}$$

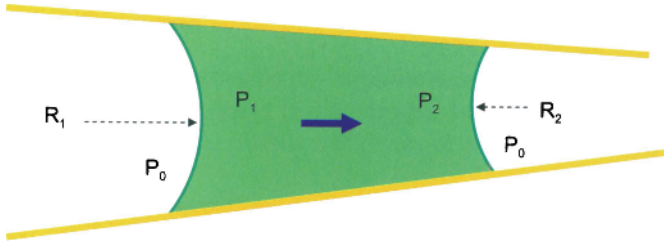

Figure 1.28 Sketch of a liquid plug moving under capillary forces between two plates. The contact angle is $\theta < 90°$.

Next, we show that $R_2 < R_1$. Looking at figure 1.29, we have

$$R_2 \sin\beta = d_2, \tag{1.42}$$

where d_2 is the half-distance between the plates at the narrower contact point. The angle β is

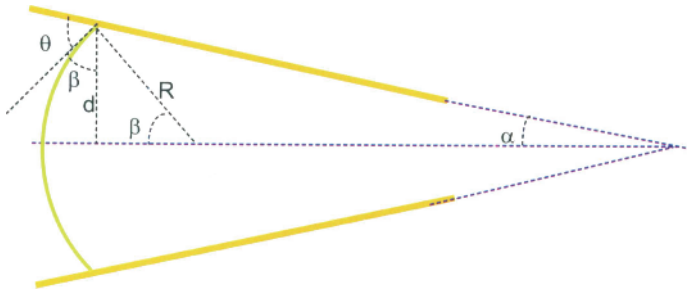

Figure 1.29 Curvature of the interface in a dihedral.

linked to θ and α by the relation

$$\beta = \frac{\pi}{2} + \alpha - \theta. \tag{1.43}$$

Finally we obtain

$$R_2 = \frac{d_2}{\cos(\alpha - \theta)}. \tag{1.44}$$

Using the same reasoning with a meniscus oriented in the opposite direction, we obtain the expression of R_1

$$R_1 = \frac{d_1}{\cos(\alpha + \theta)}. \tag{1.45}$$

Comparing relations (1.44) and (1.45), noting that $d_2 < d_1$ and $\cos(\alpha - \theta) > \cos(\alpha + \theta)$, we deduce that R_2 is then smaller than R_1, and $P_1 > P_2$. The situation is not stable. Liquid moves from the high pressure region to the low pressure region and the plug moves towards the narrow gap region. It has also been observed that the plug accelerates; it is due to the fact that the difference of the curvatures in equation (1.41) is increasing when the plug moves to a narrower region. Bouasse [24] has remarked that the same type of motion applies for a cone, where the plug moves towards the tip of the cone. In reality, Bouasse used a conical frustum (slice of cone) in order to let the gas escape during plug motion.

1.3.3.7 Laplace's Law in Medicine: Normal and Shear Stress in Blood Vessels

1.3.3.7.1 Shear Stress in Vascular Networks A human body – or any mammalian organism – respects the rules of physics. Take the example of blood vessels. The arrangement of blood vessel networks very often satisfies Murray's law (figure 1.30). In 1926, Murray observed the

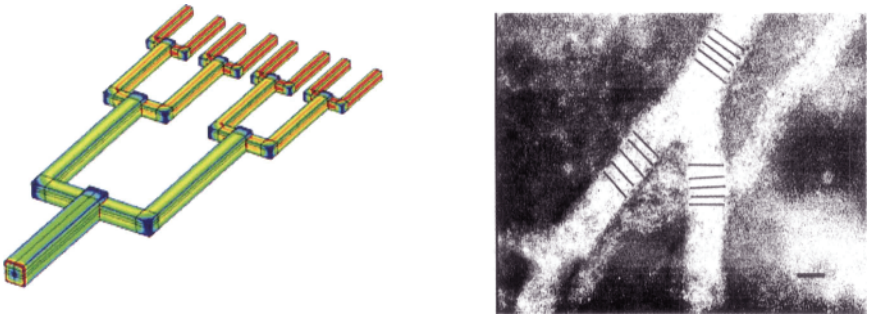

Figure 1.30 Left: Schematic of blood vessel system. Right: photograph of blood vessel division in chickens from [26].

morphology of the blood system and found a very general relation between the dimensions of a "parent" branch and of a "daughter" branch, and he found that the same relation applies at any level of bifurcation. Soon after, he published this discovery [25]. Since that time, this relation is known as Murray's law and can be written as

$$d_0^3 = d_1^3 + d_2^3, \tag{1.46}$$

where d_0, d_1, and d_2 are the "parent" and "daughters" channel diameters. Usually, daughter branches have the same dimension $d_1 = d_2$. A recurrence relation can be deduced from (1.46); it shows that the diameter, flow rates and average velocities at the n^{th} generation, i.e. at a bifurcation of rank n (figure 1.30), are related to the "origin" diameter, flow rate and average velocity by the relations

$$d_n = \frac{d_0}{2^{\frac{n}{3}}}, \tag{1.47}$$

$$Q_n = \frac{Q_0}{2^n}, \tag{1.48}$$

$$V_n = \frac{V_0}{2^{\frac{n}{3}}}. \tag{1.49}$$

These relations can be developed further to show that the wall friction is the same at each level [26,27]. This property simply stems from the expression of the shear stress of a cylindrical duct,

$$\tau_n = \frac{8\eta V_n}{d_n} = \frac{8\eta V_0}{d_0} = \tau_0. \tag{1.50}$$

Murray showed that, on a physiological point of view, such a relation minimizes the work of the blood circulation. The important thing here is that the shear stress is constant in most blood vessel networks. Now what about the normal stress?

1.3.3.7.2 Normal Stress in Vascular Networks In the particular case of human or mammalian blood systems, the normal stress is simply the internal pressure, because, to a first approximation, the flow is purely axial and there is no radial component of the velocity. It has been observed that the thickness of the walls of blood vessels satisfies Laplace's law (figure 1.31). In this particular case, the surface tension is replaced by the wall tension T, and Laplace's law becomes

$$P = \frac{T}{R}. \tag{1.51}$$

At a given distance from the heart, the pressure is approximately the same and Laplace's equation (1.51) has the consequence that the wall tension increases together with the radius. As a consequence, arteries have larger wall thickness than veins, and similarly veins compared to capillaries. In medicine, an aneurysm is a localized, blood-filled dilation (balloon-like bulge) of

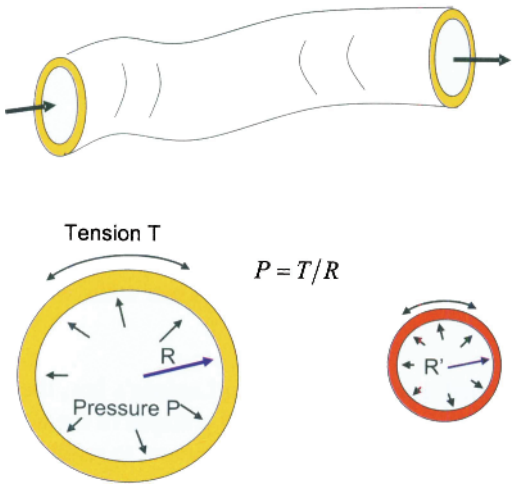

Figure 1.31 Schematic view of a blood vessel: if the internal pressure is P, the tension in the wall is $T = PR$. Small blood vessels have thinner walls than large blood vessels.

a blood vessel caused by disease or weakening of the vessel wall. Aneurysms most commonly occur in arteries at the base of the brain and in the aorta (the main artery coming out of the heart, an aortic aneurysm). It has been observed that, as the size of an aneurysm increases, there is an increased risk of rupture, which can result in severe hemorrhage, other complications or even death. This expansion is a direct consequence of the preceding reasoning: if the thickness of the vascular wall is such as it withstands a given tension T, an increase of the radius will require a higher tension of the wall, and therefore the aneurysm will continue to expand until it ruptures (figure 1.32). A similar logic applies to the formation of diverticuli in the gut [28].

1.3.3.8 Laplace's Law in Medicine: the Example of Lung Alveoli

It is very tempting to refer automatically to Laplace's law because of its simplicity. But one should refrain from doing that uncritically. A striking example is that of lung ventilation. Ventilation of lungs has been widely studied for medical purposes. It was usual to consider the alveoli such as spherical balloons inflated during lung ventilation (fig. 1.33). The problem is

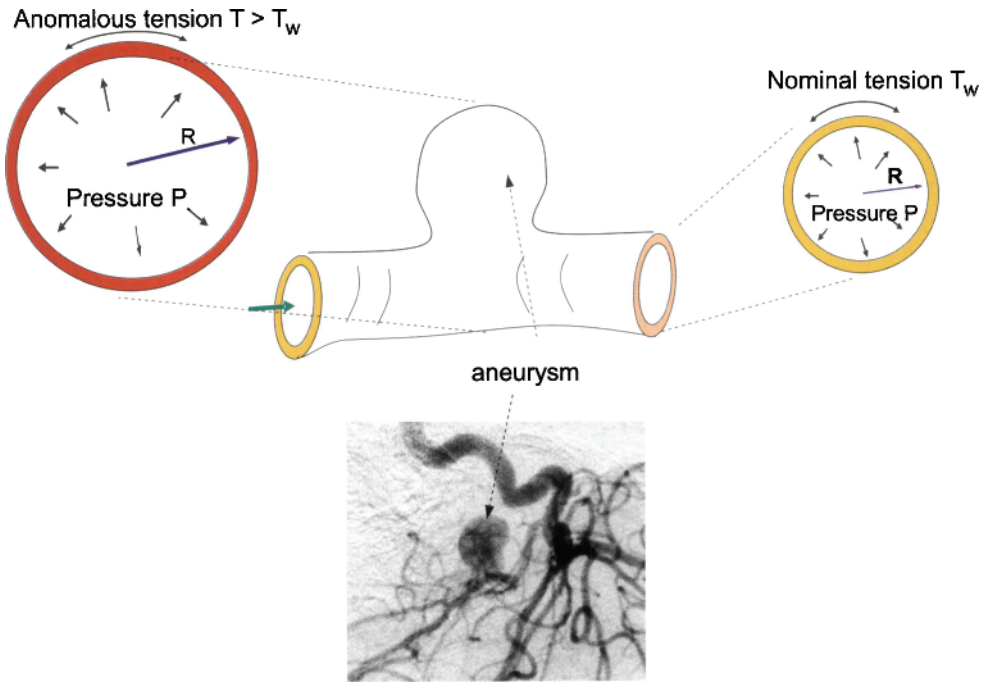

Figure 1.32 Sketch of an aneurysm. The wall tension required at the location of the aneurysm exceeds the wall tension that the thickness of the wall can withstand.

that the alveoli are connected, and when applying Laplace's law, the air in the smaller alveoli should be driven to the larger alveoli and a general collapse of the lungs would occur. Because the collapse of the alveoli does not – luckily – correspond to reality, it has been suggested that the concentration of surfactant in the alveoli is not uniform and compensates for the different pressures. Recently, a different, more realistic analysis has been made [29]: the alveoli are not

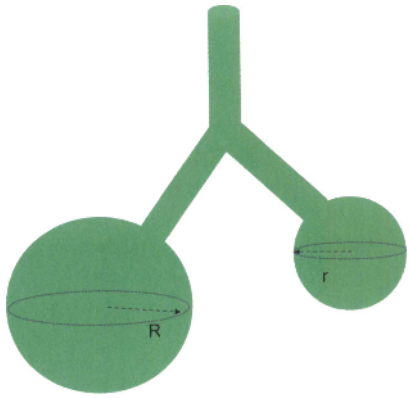

Figure 1.33 Wrong sketch for the alveoli leading to an improper application of Laplace's law.

"free" spheres but are packed together (figure 1.34) and there are pores in the alveoli walls.

Alveoli cannot expand freely, and they are limited in their inflation. As a result, smallest alveoli do not collapse during ventilation, because large alveoli cannot grow indefinitely, and Laplace's law is not the answer in this kind of problem.

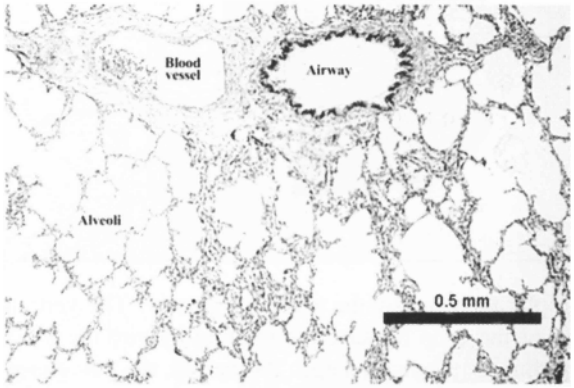

Figure 1.34 Image of lung alveoli; Detail from an original slide generously provided by A. Mescher.

1.3.3.9 Laplace's Law in a Gravity Field

Consider a drop on a flat horizontal surface, a drop large enough that gravity deforms it. For simplicity, let us assume a liquid droplet of density ρ in a free atmosphere. Inside the liquid, this hydrostatic pressure is given by the term $P_1 = const - \rho gz$, where z is the vertical direction oriented upwards, and outside the drop the atmospheric pressure can be considered constant, $P_2 = const$. The Laplace law is then

$$\gamma\left(\frac{1}{R_1}+\frac{1}{R_2}\right) = const - \rho gz. \tag{1.52}$$

The curvature is then smaller at the top of the drop than it is at the bottom of the drop. This effect can well be seen in an Evolver simulation (figure 1.35).

1.3.3.10 Generalization: Laplace's Law in Presence of a Flow Field

The expression of Laplace's law derived in section 1.3 assumed totally static conditions, or at the least that the shear rate of the flow field close to the interface is negligible in comparison with the surface tension. This is indeed often the case since usually capillary numbers are small in microfluidic systems. Recalled that the capillary number is a non-dimensional number characterizing the ratio between inertial forces and capillary forces. However, the flow field effect on the interface cannot be always neglected. For example, systems like flow-focusing devices are currently used in biotechnology to produce emulsions and encapsulates [30-32]. In such systems, the dynamic flow field exerts a considerable force on the interface, as has been shown by Tan et al. [33] (figure 1.36). In such a case the balance of the forces on the surface is more complicated: the complete stress tensor has to be taken into account, and we obtain the generalized Laplace law for liquid 1 and 2:

$$(P_1 - P_2)n_i = \gamma\left(\frac{1}{R_1}+\frac{1}{R_2}\right)n_i + \left(\sigma'^{(1)}_{ik} - \sigma'^{(2)}_{ik}\right)n_k, \tag{1.53}$$

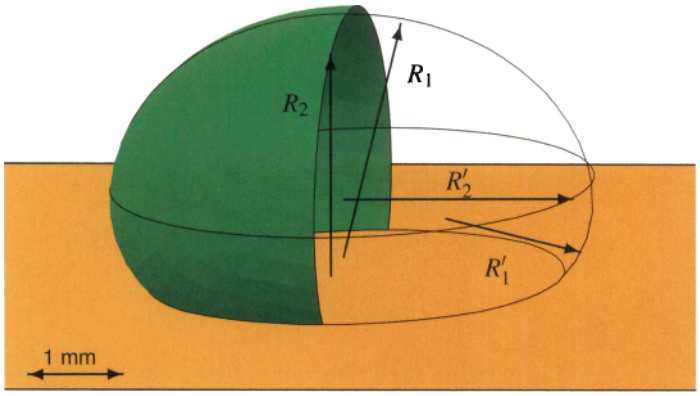

Figure 1.35 Large droplet flattened by the action of gravity: The vertical curvature radius R_1' is small at the bottom of the drop because the internal hydrostatic pressure is larger and the horizontal curvature radius R_2' relatively large. At the top, the curvatures R_1 and R_2 are equal and relatively large.

where n_i is the unit normal vector, and σ_{ik}' the viscous part of the stress tensor [34]. Note the implicit summation on the repeated index k on the right side of (1.53).

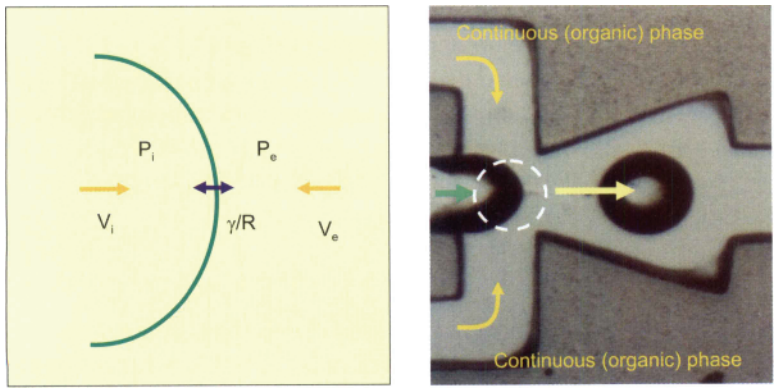

Figure 1.36 Left: sketch of the interface; right: photo of a flow focusing device; the generalized Laplace's law applies for the incoming discontinuous phase (inside the dotted circle).

1.3.4 Wetting - Partial or Total Wetting

So far, we have dealt with interfaces between two fluids. Triple contact lines are the intersections of three interfaces involving three different materials: for example a droplet of water on a solid substrate in an atmosphere has a triple contact line. Liquids spread differently on a horizontal plate according to the nature of the solid surface and that of the liquid. In reality, it depends also on the third constituent, which is the gas or the fluid surrounding the drop. Two different situations are possible: either the liquid forms a droplet, and the wetting is said to be partial, or the liquid forms a thin film wetting the solid surface, the horizontal dimension of the film depending on the initial volume of liquid (figure 1.37). For example, water spreads like a film

on a very clean and smooth glass substrate, whereas it forms a droplet on a plastic substrate. In the case of partial wetting, there is a line where all three phases come together. This line is called the contact line or the triple line.

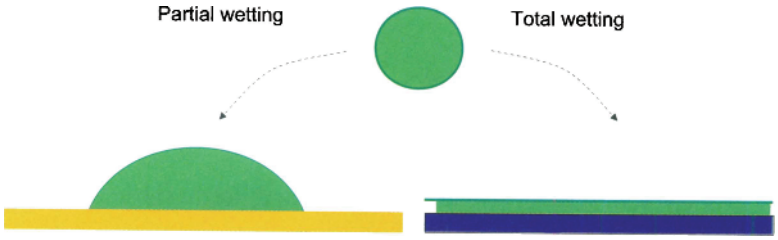

Figure 1.37 Wetting is said to be total when the liquid spreads like a film on the solid surface.

A liquid spreads on a substrate in a film if the energy of the system is lowered by the presence of the liquid film (figure 1.38). The surface energy per unit surface of the dry solid surface is γ_{SG}; the surface energy of the wetted solid is $\gamma_{SL}+\gamma_{LG}$. The spreading parameter S determines the type of spreading (total or partial)

$$S = \gamma_{SG} - (\gamma_{SL} + \gamma_{LG}). \tag{1.54}$$

If $S > 0$, the liquid spreads on the solid surface; if $S < 0$ the liquid forms a droplet.

Figure 1.38 Comparison of the energies between the dry solid and the wetted solid.

When a liquid does not totally wet the solid, it forms a droplet on the surface. Two situations can occur: if the contact angle with the solid is less than 90°, the contact is said to be "hydrophilic" if the liquid has a water base, or more generally "wetting" or "lyophilic". In the opposite case of a contact angle larger than 90°, the contact is said to be "hydrophobic" with reference to water or more generally "not wetting" or "lyophobic" (figure 1.39 and figure 1.40).

1.3.5 Contact Angle - Young's Law

1.3.5.1 Young's Law

We have seen that surface tensions are not exactly forces, their unit is N/m; however they represent a force that is exerted tangentially to the interface. Surface tension can be looked at as a force per unit length. This can be directly seen from its unit. But it may be interesting to give a more physical feeling by making a very simple experiment (figure 1.41) [22]. Take a solid frame and a solid tube that can roll on this frame. If we form a liquid film of soap between the frame and the tube – by plunging one side of the structure in a water-soap solution – the tube starts to move towards the region where there is a liquid film. The surface tension of the liquid

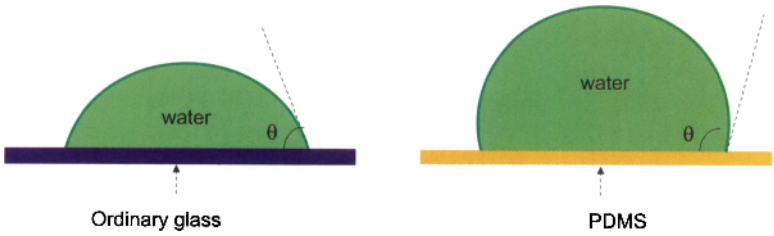

Figure 1.39 Water spreads differently on different substrate.

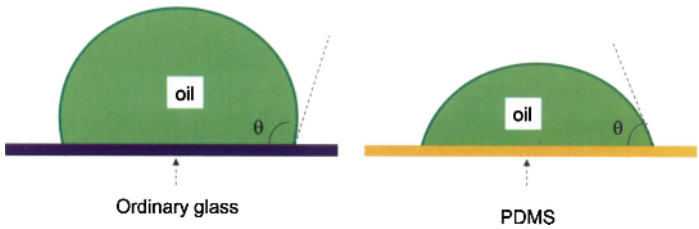

Figure 1.40 Silicone oil has an opposite wetting behavior than water.

film exerts a force on its free boundary. On the other hand, we can increase the film surface by exerting a force on the tube. The work of this force is given by both of the relations

$$\delta W = F dx, \qquad \delta W = \gamma dA = 2\gamma L dx. \tag{1.55}$$

The coefficient 2 stems from the fact that there are two interfaces between the liquid and the air, on either side of the film. Comparing these relations shows that the surface tension γ is a force per unit length, perpendicular to the tube, in the plane of the liquid and directed towards the liquid.

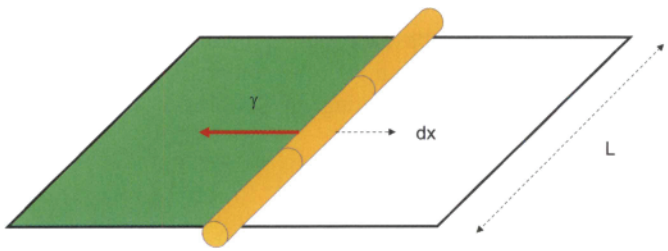

Figure 1.41 A tube placed on a rigid frame whose left part is occupied by a soap film requires a force to be displaced towards the right, this force opposed to the surface tension that tends to bring the tube to the left.

We can then sketch the different forces that are exerted by the presence of a fluid on the triple line (figure 1.42). At equilibrium, the resultant of the forces must be zero. We use a coordinate

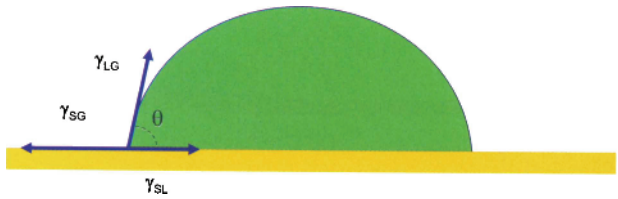

Figure 1.42 Schematic of the forces at the triple contact line.

system where the x-axis is the tangent to the solid surface at the contact line (horizontal) and the y-axis is the direction perpendicular (vertical). At equilibrium, the projection of the resultant on the x-axis is zero and we obtain the relation

$$\gamma_{LG}\cos\theta = \gamma_{SG} - \gamma_{SL}. \tag{1.56}$$

This relation is called Young's law and is very useful to understand the behavior of a drop. Especially, it shows that the contact angle is determined by the surface tensions of the three constituents. For a droplet on a solid, the contact angle is given by the relation

$$\theta = \arccos\left(\frac{\gamma_{SG} - \gamma_{SL}}{\gamma_{LG}}\right). \tag{1.57}$$

Young's law can be more rigorously derived from free energy minimization. Consider a sessile droplet large enough for the effect of the triple line to be neglected. The change of free energy due to a change in droplet size can be written as [30]

$$dF = \gamma_{SL}dA_{SL} + \gamma_{SG}dA_{SG} + \gamma_{LG}dA_{LG} = (\gamma_{SL} - \gamma_{SG} + \gamma_{LG}\cos\theta)dA_{SL}, \tag{1.58}$$

where θ is the contact angle. At mechanical equilibrium $dF = 0$ and

$$\gamma_{SL} - \gamma_{SG} + \gamma_{LG}\cos\theta = 0. \tag{1.59}$$

Equation (1.59) is Young's law, identical to (1.56).

Note that sometimes it happens that, in real experimental situations when we deal with real biological liquids, one observes unexpected changes in the contact angle with time. This is just because biological liquids are inhomogeneous and can deposit a layer of chemical molecules on the solid wall, thus progressively changing the value of the tension γ_{SL}, and consequently the value of θ, as stated by Young's law.

1.3.5.2 Droplet on a Cantilever

Let us come back to the derivation of Young's law. Young's law has been obtained by a projection on the x-axis of the surface tension forces. But the force balance applies also to projection in any direction. We will mention two cases where slanted projection of Young's law is of importance, first that of a cantilever, second that of the contact between three liquids. In the case of a micro-cantilever, the presence of a droplet induces capillary forces along the triple line (figure 1.43). The deformation results from the resultant of the capillary forces perpendicular to the cantilever. At rest, this resultant bends the cantilever. The calculation is lengthy and has been derived by Yu and Zhao [35].

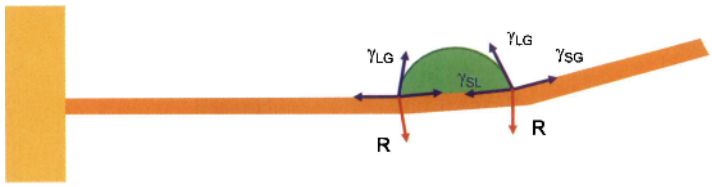

Figure 1.43 Cantilever deformed by the presence of a water droplet, after [35].

1.3.5.3 Contact Between Three Liquids – Neumann's Construction

Take two immiscible liquids, denoted 1 and 2, with the droplet of liquid 2 deposited on the interface between liquid 1 and a gas. Even if the density of liquid 2 is somewhat larger than that of liquid 1, the droplet may "float" on the surface, as shown in figure 1.44. The situation is comparable to that of Young's law with the difference that the situation is now two-dimensional. It is called Neumann's construction, and the following vector equality holds:

$$\vec{\gamma}_{L1L2} + \vec{\gamma}_{L1G} + \vec{\gamma}_{L2G} = 0. \tag{1.60}$$

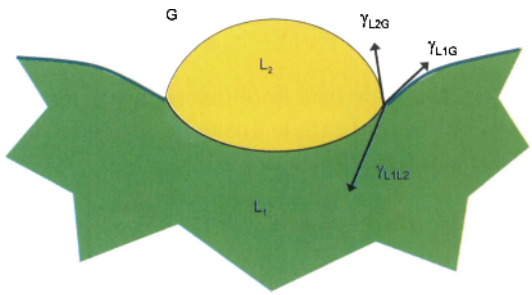

Figure 1.44 Droplet on a liquid surface.

Note that the densities of the two liquids condition the vertical position of the center of mass of the droplet, but at the triple line, it is the y-projection of equation (1.60) that governs the morphology of the contact. In figure 1.45 we show some pictures of floating droplets obtained by numerical simulation (Surface Evolver).

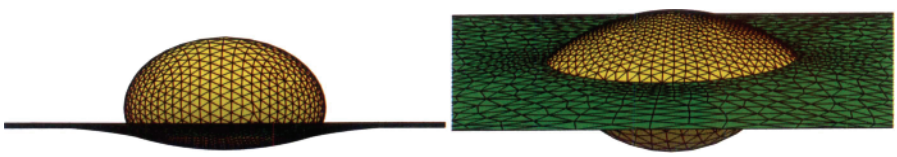

Figure 1.45 Numerical simulations of different positions of a droplet (1 mm) on a liquid surface depending on the three surface tensions. Left: the liquid/liquid surface tension is very large. Right: the surface tension of the droplet with the other liquid has been reduced. Both drops are at equilibrium due to the balance of buoyancy and surface tensions.

1.3.5.4 Nanobubbles on Hydrophobic Walls, Line Tension and the Modified Young Law

It has been observed that bubbles often form along hydrophobic walls, even when the surface is smooth. The size of these bubbles is in the mesoscopic range – between the microscopic and nanoscopic scales: bubble dimension is usually less than 200 nm. A paradox arises when calculating the internal pressure. Using the Laplace law with a curvature radius of the order of the observed contact at the wall, one finds that the internal pressure should be of the order of

$$P \simeq \frac{\gamma}{R} \simeq \frac{70 \times 10^{-3}}{200 \times 10^{-9}} \simeq 3.5 \times 10^{5} Pa. \tag{1.61}$$

At this level of pressure the gas should dissolve, and the bubble would disappear rapidly in the liquid. So why are these bubbles stable? From a Laplace's law point of view, either their surface tension should be smaller than that of a "macroscopic" bubble, or their curvature radius should be larger. It is easy to see that a reduced surface tension is not sufficient to find a sustainable internal pressure. On the other hand, at this scale, contact angle measurements are very tricky. However, recent measurements [36] have shown that nano-bubbles have very flat profiles – the base radius is 5-20 times larger than the height – because the contact angle of the bubble is much smaller than a macroscopic contact angle of the bubble on the same substrate (figure 1.46).

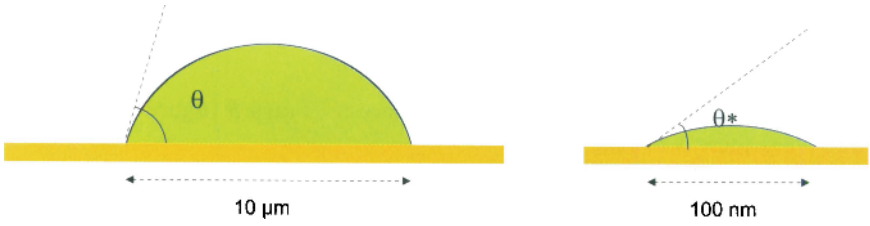

Figure 1.46 Comparative sketches of micro-bubble and nano-bubble (not to scale).

The problem has now shifted from Laplace's law to Young's law. What has changed in Young's law for the contact angle between the nanoscale and the microscopic/macroscopic scale? The answer to this question is not yet clear. A plausible answer is connected to the notion of "line tension" and to the so-called modified Young's law. Young's law has been derived for a triple line without consideration of the interactions near the triple contact line. A sketch of the interactions leading to surface tension and line tension is shown in figure 1.47. The molecules close to the triple line experience a different set of interactions than at the interface. To take into account this effect, a line tension term can be introduced in Young's law [37,38]:

$$\gamma_{SG} = \gamma_{SL} + \gamma_{LG} \cos\theta + \frac{\gamma_{SLG}}{r}, \tag{1.62}$$

where r is the contact radius, γ_{SLG} the line tension (unit N), and θ^* the real contact angle. The contact angle is then changed by the line tension according to

$$\cos\theta^* = \cos\theta - \frac{\gamma_{SLG}}{r\gamma_{LG}}. \tag{1.63}$$

For a droplet contact radius larger than 10 μm, the effect of the line tension is negligible; the value of the correction term is of the order of 10^{-4} [22]. But this is not the case for nano-drops and nano-bubbles, whose contact radii are much smaller.

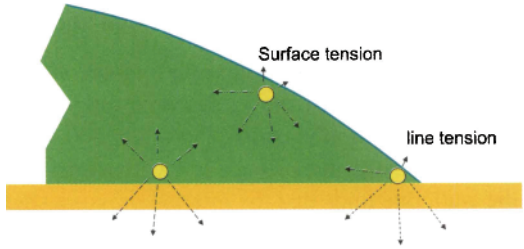

Figure 1.47 Sketch of interactions leading to surface tension and line tension.

1.3.6 Work of Adhesion, Work of Cohesion and the Young-Dupré Equation

In this section, we introduce the notions of work of adhesion and work of cohesion. These notions are valid for solids or immiscible liquids. When applied to a solid and a liquid, the concept of work of adhesion combined with Young's law produces the Young-Dupré equation. Work of adhesion and Young-Dupré's equation have been widely used to determine the surface tension of solids (section 1.4.3).

1.3.6.1 Work of Adhesion

Imagine a body contacting another body on a surface S of area S (figure 1.48). The surface energy of S when there is contact is

$$E_{12} = \gamma_{12} S. \tag{1.64}$$

The work of adhesion is the work required to separate the two bodies. After separation, the surface energies are

$$E = E_1 + E_2 = (\gamma_1 + \gamma_2) S. \tag{1.65}$$

The work of adhesion is then

$$W_a = \gamma_1 + \gamma_2 - \gamma_{12}. \tag{1.66}$$

1.3.6.2 Work of Cohesion

The work of cohesion is obtained similarly, but this time the body being split is homogeneous (figure 1.49). The same reasoning yields

$$W_c = 2\gamma_1. \tag{1.67}$$

In other words, the surface energy is half the work of cohesion.

1.3.6.3 The Young-Dupré Equation

Let us express the work of adhesion for a liquid and a solid (figure 1.50). Using (1.66) with the surface tensions $\gamma_1 = \gamma_{LG} = \gamma$, $\gamma_2 = \gamma_{SG}$, and $\gamma_{12} = \gamma_{SL}$, we obtain

$$W_a = \gamma + \gamma_{SG} - \gamma_{SL}. \tag{1.68}$$

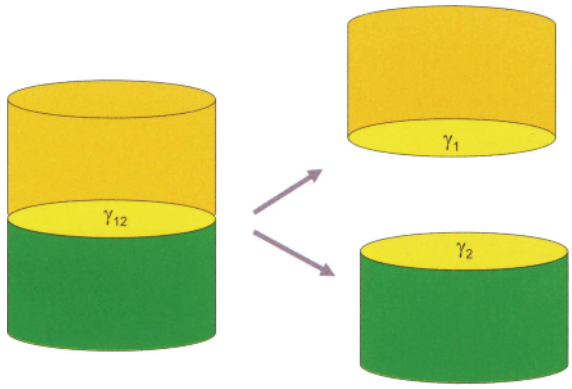

Figure 1.48 Work of adhesion is the work done to separate two surfaces of incompatible substance.

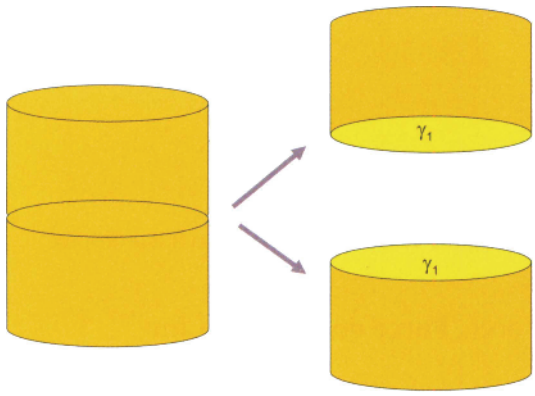

Figure 1.49 Work of cohesion is the work done to separate two surfaces of the same substance.

Upon substitution of Young's law, we derive the Young-Dupré equation

$$W_a = \gamma(1 + \cos\theta). \tag{1.69}$$

For a super-hydrophobic contact, $\theta = \pi$ and $\cos\theta = -1$; we deduce that $W_a = 0$: there is no work needed to separate a super-hydrophobic liquid from a solid. Concretely, a droplet of water rolls freely over a super-hydrophobic surface. The Young-Dupré equation indicates that the more hydrophobic (non-wetting) is the contact between a liquid and a solid, the smaller is the work of adhesion.

On the other hand, adhesion maintains a droplet suspended below a solid, as shown in figure 1.51.

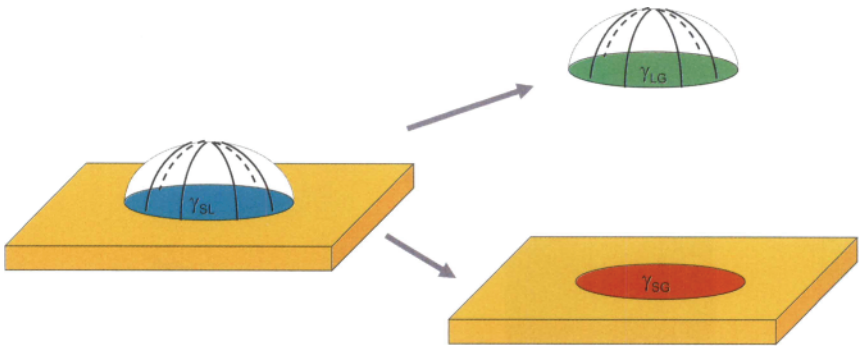

Figure 1.50 Sketch of the Young-Dupré equation for the work of adhesion of a liquid and a solid: $W_a = \gamma(1+\cos\theta)$.

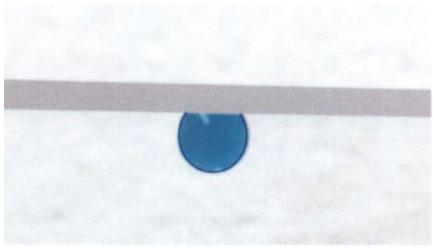

Figure 1.51 Sketch of a suspended droplet.

1.3.7 Capillary Force, Force on a Triple Line

1.3.7.1 Introduction

We have seen in section 1.3.5 the correspondence between surface tension and capillary forces. One example is that of a coin floating on water. Figure 1.52 shows a small coin floating on water, even if the buoyancy forces are not sufficient to maintain it at the water surface. The capillary forces all along the edge of the coin add a supplementary vertical force which counterbalances the apparent weight of the coin.

Capillary forces are still more important at a micro-scale. We have all seen insects "walking" on the surface of a water pond (figure 1.53). Their hydrophobic legs do not penetrate the water surface and their weight is balanced by the surface tension force. More than that, it is observed that some insects can walk up a meniscus, i.e. can walk on an inclined water surface. The explanation of this phenomenon was recently given by Hu *et al.* [39] and refers to complex interface deformation under capillary forces.

In the domain of microfluidics, capillary forces are predominant; some examples of the action of capillary forces are given in the following sections.

1.3.7.2 Capillary Force Between Two Parallel Plates

We all have remarked that two parallel plates squishing a liquid film make the plates very adhesive. For instance, when using a microscope to observe objects in a small volume of liquid deposited on a plate and covered by a secondary glass plate, it is very difficult to separate the plates. We sketch this problem in figure 1.54. We will assume the liquid does not reach the

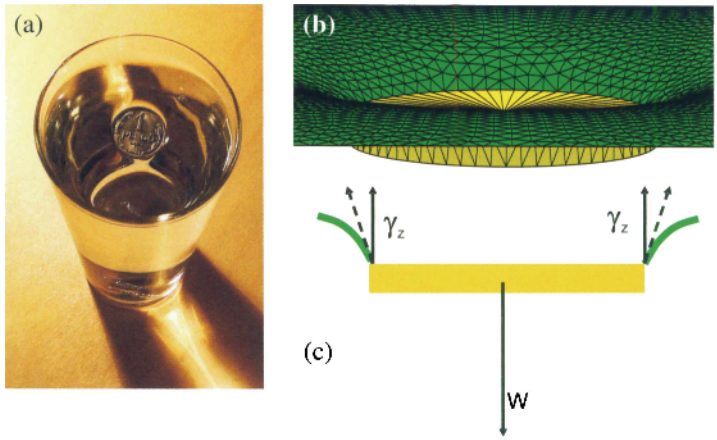

Figure 1.52 A small coin floats on water, even though the buoyancy forces are not sufficient to maintain it at the water surface (a). Surface tension forces act on the coin edge to counterbalance gravity: (b) Surface Evolver simulation and (c) sketch of the forces.

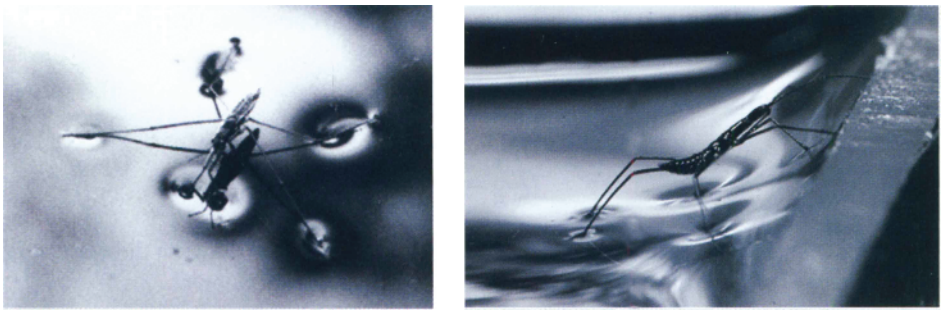

Figure 1.53 Left: Capillary forces make the water surface resist the weight of an insect. Right: an insect walking up a meniscus. Reprinted with permission from [33], ©Nature Journal, 2005.

plate edges, for simplicity. First we remark that the meniscus has a circular shape horizontally, radius R, in order to minimize the free energy.

Figure 1.54 Film of water between two glass plates.

We use Laplace's law at the free interface. The first (horizontal) radius of curvature is approximately R. The second (vertical) radius of curvature, shown in figure 1.55, is calculated

by

$$R_2 \sin\left(\frac{\pi}{2} - \theta\right) = \frac{h}{2}, \tag{1.70}$$

or

$$R_2 = \frac{h}{2\cos\theta}. \tag{1.71}$$

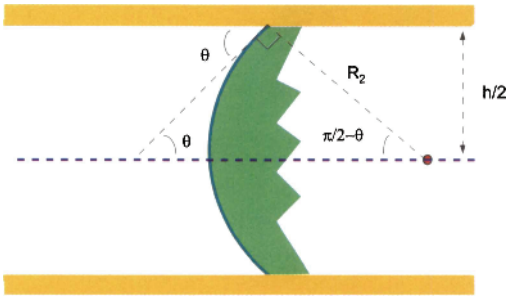

Figure 1.55 Calculation of the vertical curvature.

Laplace's law states that

$$\Delta P = \gamma\left(\frac{1}{R} - \frac{2\cos\theta}{h}\right). \tag{1.72}$$

In (1.72), the minus sign derives from the concavity of the interface. Because the vertical gap h is much less than the horizontal dimension R, we have the approximation

$$\Delta P \simeq -\frac{2\gamma\cos\theta}{h}. \tag{1.73}$$

And the capillary force that links the plates together is

$$F \simeq \frac{2\gamma\cos\theta}{h}\pi R^2. \tag{1.74}$$

This capillary force can be quite important; for $h = 10\ \mu$m and $R = 1$ cm, the force F is of the order of 2.5 N.

1.3.7.3 Capillary Rise in a Tube

When a capillary tube is plunged into a volume of wetting liquid, the liquid rises inside the tube under the effect of capillary forces (figures 1.56 and 1.57). It is observed that the height reached by the liquid is inversely proportional to the radius of the tube.

Historically, many scientists have investigated this phenomenon, from Leonardo da Vinci, to Hauksbee, to Jurin. This property is now referred to as Jurin's law [40]. Using the principle of minimum energy, one can conclude that the liquid goes up in the tube if the surface energy of the dry wall is larger than that of the wetted wall. We define the impregnation criterion I by

$$I = \gamma_{SG} - \gamma_{SL}. \tag{1.75}$$

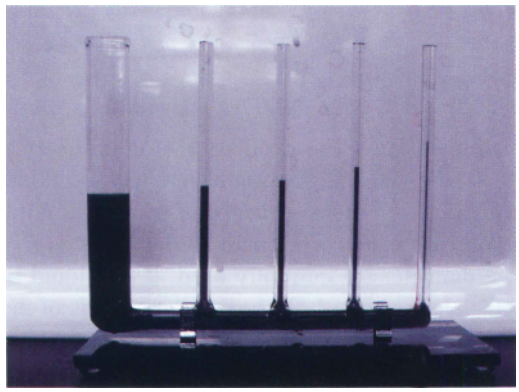

Figure 1.56 Capillary rise in tubes of different internal cross section.

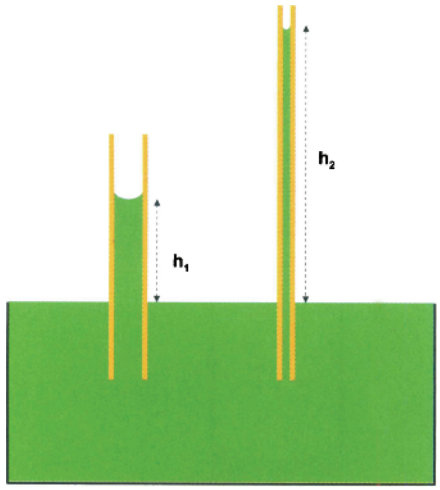

Figure 1.57 Capillary rise is inversely proportional to the capillary diameter.

The liquid rises in the tube if $I > 0$, else the liquid descends in the tube. Using Young's law, the impregnation criterion can be written in the form

$$I = \gamma \cos\theta. \tag{1.76}$$

When the liquid rises in the tube, the system gains gravitational potential energy – because of the elevation of a volume of liquid – and loses capillary energy due to the reduction of the surface energy. The balance is [22]

$$E = \frac{1}{2}\rho g h V_{liquid} - S_{contact} I = \frac{1}{2}\rho g h(\pi R^2 h) - 2\pi R h I = \frac{1}{2}\rho g \pi R^2 h^2 - 2\pi R h \gamma \cos\theta. \tag{1.77}$$

Note that we have not taken into account in (1.77) the detailed shape of the meniscus for the height h. The equilibrium elevation of the liquid is given by

$$\frac{\delta E}{\delta h} = 0, \tag{1.78}$$

which results in

$$h = \frac{2\gamma\cos\theta}{\rho g R} = 0, \tag{1.79}$$

Equation (1.79) is called Jurin's law. The capillary rise is inversely proportional to the tube radius. Jurin's law can also be applied to the case where the liquid level in the tube decreases below the outer liquid surface; this situation happens when $\theta > 90$ degrees. The maximum possible height that a liquid can reach corresponds to $\theta = 0$ and is $h = \frac{2\gamma}{\rho g R}$. In microfluidics, capillary tubes of 100 μm diameter are currently used; if the liquid is water ($\gamma = 72$ mN/m), and using the approximate value $\cos\theta \approx 1/2$, the capillary rise is of the order of 14 cm, which is quite important at the scale of a microcomponent. We have just given an expression for the capillary rise and we have seen that the capillary rise is important. What is the corresponding capillary force? The capillary force balances the weight of the liquid in the tube. This weight is given by

$$F = \rho g \pi R^2 h. \tag{1.80}$$

Replacing h by its value from equation (1.79), we find the capillary force

$$F = 2\pi R\gamma\cos\theta. \tag{1.81}$$

The capillary force is the product of the length of the contact line $2\pi R$ times the line force $f = \gamma\cos\theta$. This line force is sketched in figure 1.58.

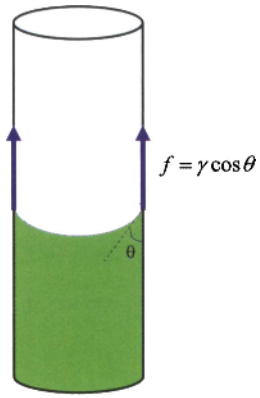

Figure 1.58 Sketch of the capillary force of a liquid inside a tube.

Note that the capillary force per unit length f is identical to the impregnation criterion

$$f = \gamma\cos\theta = I. \tag{1.82}$$

For $f > 0$ the liquid goes up in the tube and for $f < 0$ the liquid goes down. Note that figure 1.58 is not quite exact: the liquid surface outside the tubes is not totally horizontal. There are also capillary forces on the outside of the tube, as shown in figure 1.59. To derive the expression of the capillary rise inside the tube, a control volume corresponding to the liquid volume inside the tube was first considered. Let us consider now a control volume defined by the pipette (figure 1.60). The force to maintain the pipette is

$$F = P - P_A + P_{c,e} + P_{c,i}, \tag{1.83}$$

where P is the weight of the tube, P_A the floatation force and $P_{c,i}$ and $P_{c,e}$ are respectively the interior and exterior capillary forces exerted on the solid.

$$F = P - P_A + 2\pi R_{int}\gamma\cos\theta + 2\pi R_{ext}\gamma\cos\theta. \tag{1.84}$$

This force is a function of the surface tension γ. In section 1.4, we will see that the measure of such a force constitutes a way to determine the surface tension.

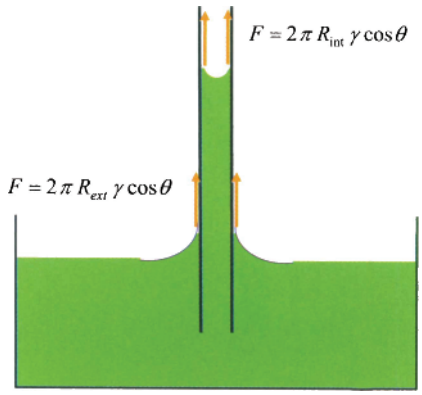

Figure 1.59 Capillary forces act also on the tube exterior, raising the level of the liquid around the tube (if the liquid wets the solid; it would be the opposite if the liquid were not wetting).

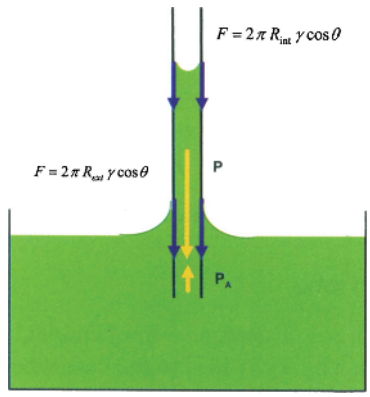

Figure 1.60 Forces acting on the pipette.

1.3.7.4 Capillary Rise Between Two Parallel Vertical Plates

The same reasoning can be done for a meniscus rising between two vertical parallel plates (figure 1.61) separated by a distance $d = 2R$. It is easy to show that in this case

$$h = \frac{\gamma\cos\theta}{\rho g R} = 0. \tag{1.85}$$

If we introduce the capillary length κ defined by

$$\kappa^{-1} = \sqrt{\frac{\gamma}{\rho g}}, \tag{1.86}$$

we can rewrite (1.86) in the form

$$h = \kappa^{-2} \frac{\cos\theta}{R} = 0, \tag{1.87}$$

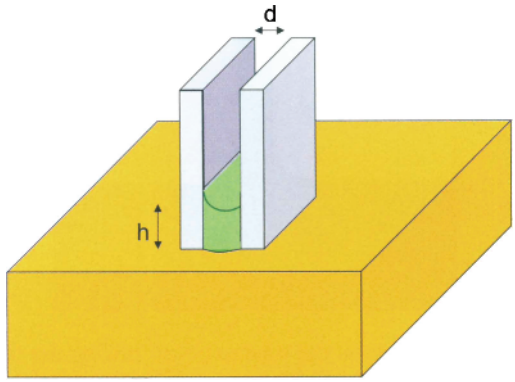

Figure 1.61 Capillary rise between two parallel vertical plates.

Remark: The expressions for the two geometries (cylinder and two parallel plates) are similar. If we use the coefficient c, with $c = 2$ for a cylinder and $c = 1$ for parallel plates [41], we have

$$h = c\kappa^{-2} \frac{\cos\theta}{R} = 0, \tag{1.88}$$

where R is either the radius of the cylinder or the half-distance between the plates.

1.3.7.5 Capillary Rise in a Pipette

The analysis of the capillary rise – or descent – in cylindrical tubes or between two parallel plates has been recently extended by Tsori [41] to the case where the walls are not parallel, as for instance a conical pipette (figure 1.62).

The mechanical equilibrium states that the Laplace pressure is balanced by the hydrostatic pressure

$$P_0 + \frac{c\gamma}{r} = P_0 - \rho g h, \tag{1.89}$$

where c is the index defined previously, $c = 2$ for cones and $c = 1$ for wedges, and r is the curvature radius of the meniscus. Note that the depth h is counted negatively from the surface. Using the same approach as that of section 1.3.3.6, the curvature radius is expressed by

$$r(h) = -\frac{R(h)}{\cos(\theta + \alpha)}, \tag{1.90}$$

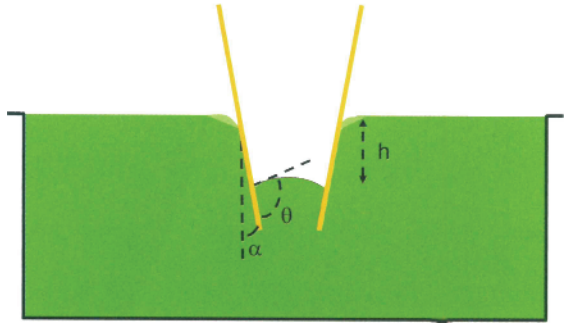

Figure 1.62 Capillary descent inside a hydrophobic conical pipette.

with

$$R(h) = R_0 + h\tan\alpha, \tag{1.91}$$

where R_0 is the internal radius of the pipette at $h = 0$. Substituting (1.91) in (1.90) and then in (1.89), we obtain

$$\cos(\theta+\alpha) = -\frac{1}{c}h(R_0 + h\tan\alpha)\frac{\rho g}{\gamma}. \tag{1.92}$$

Using the capillary length κ^{-1} to scale the variables, we obtain the non-dimensional variables $\bar{R} = \kappa R$ and $\bar{h} = \kappa h$. Equation (1.92) then becomes

$$(\tan\alpha)\bar{h}^2 + \bar{R}_0\bar{h}c\cos(\theta+\alpha) = 0. \tag{1.93}$$

This is a quadratic equation in $\bar{h}$. The discussion of this equation is somewhat complex. Depending on the values of α and θ, the meniscus may be stable or not stable; in the latter case, the meniscus jumps to the top or the bottom of the pipette, where it gets stabilized by pinning (anchoring to an angle). The diagram of figure 1.63 summarizes the meniscus behavior.

The important information here is that there are two domains where the meniscus "jumps" inside the pipette until it finds a pinning edge. The first case is that of a cone/wedge angle α larger than a critical value α^* (and the contact angle θ sufficiently large); the meniscus stays pinned at the bottom of the pipette, and no liquid penetrates the pipette, unless a negative pressure is established. On the other hand, when the angles α and θ are sufficiently small (α smaller than a negative critical value $-\alpha^*$), the liquid jumps to the top of the cone/wedge. The critical values depend on the internal radius R_0 of the pipette at $h = 0$. In conclusion, a cone-shaped micro-pipette dipped into a liquid does not have always the expected behavior, i.e. there might not be the expected capillary rise.

1.3.7.6 Force on a Triple Line

The analysis of the capillary rise in tubes has shown the expression of the capillary force on the triple contact line [42]. This expression can be generalized to any triple contact line [43]. For a triple contact line Ω – as sketched in figures 1.64 and 1.65 – the capillary force is

$$F_x = \int_\Omega \vec{f}\cdot\vec{i}\,dl = \int_\Omega \gamma\cos\theta\,\vec{n}\cdot\vec{i}\,dl. \tag{1.94}$$

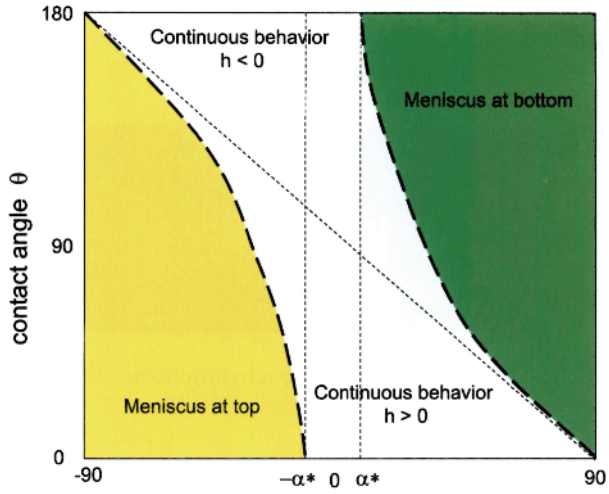

Figure 1.63 Diagram of meniscus behavior in the (θ, α) plane. The angle α^* is defined by $\sin\alpha^* = \frac{R_0^2}{4c}$. Depending on the contact angle, if the angle of a pipette is sufficiently large, whether it is hydrophobic or hydrophilic, the meniscus will stay at the bottom. No liquid will penetrate the pipette unless a negative pressure is established in the pipette.

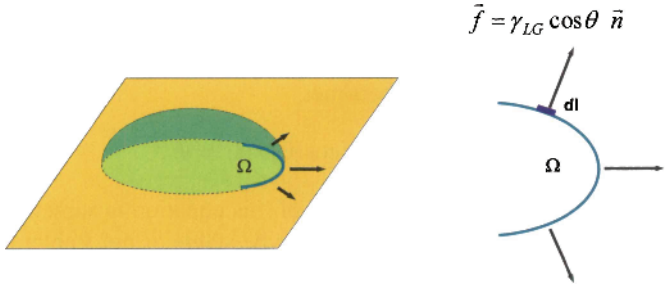

Figure 1.64 Schematic of the capillary force on a triple line.

Suppose that we want to find the value of the resultant of the capillary forces in a particular direction, say the x-direction. The projection along the x-direction of equation (1.90) can be written as

$$F_x = \int_\Omega \vec{f} \cdot \vec{i}\, dl = \int_\Omega \gamma \cos\theta \vec{n} \cdot \vec{i}\, dl. \tag{1.95}$$

Equation (1.95) can be simplified and cast in the form

$$F_x = \int_\Omega \gamma \cos\theta \, \vec{n} \cdot \vec{i}\, dl = \gamma \cos\theta \int_\Omega \vec{n} \cdot \vec{i}\, dl = \gamma \cos\theta \int_\Omega \cos\alpha\, dl = \gamma \cos\theta \int_0^e dl'. \tag{1.96}$$

Finally we obtain the expression

$$F_x = e\gamma \cos\theta. \tag{1.97}$$

Equation (1.97) shows that the resulting force on a triple contact line in any direction does not depend on the shape of the interface [43]; it depends only on the distance between the two ends of the triple line normal to the selected direction.

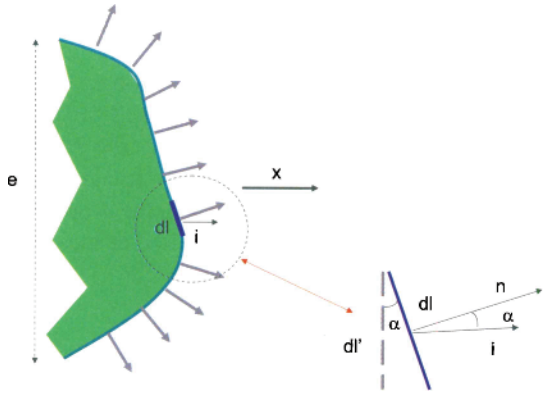

Figure 1.65 Capillary force on a triple contact line in the x-direction.

1.3.7.7 Examples of Capillary Forces in Microsystems

It is very common in biotechnology to use plates comprising thousands of micro-holes or cusps. The position of the free surface of the liquid in the cusps is of utmost importance. In particular, the liquid must not exit the holes under the action of capillary forces. As an example, figure 1.66 shows a free liquid interface in a square hole, calculated with the Surface Evolver. In the following Chapter, we will study in more detail the position of an interface in a hole, as a function of the wetting characteristics of the solid surfaces and the shape of the hole.

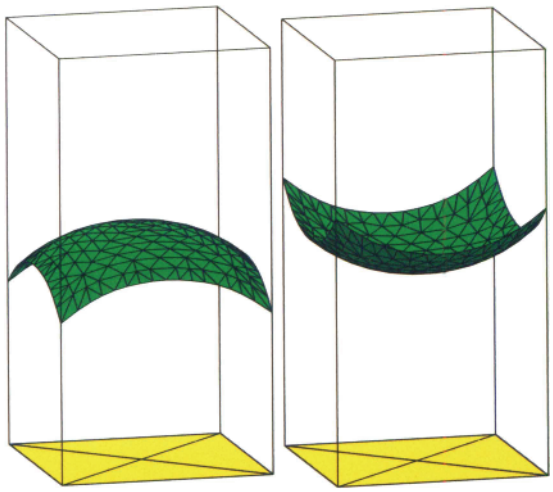

Figure 1.66 The surface of a liquid in a micro-well is not flat due to capillary forces. The figure is a simulation with the Surface Evolver. Left: case of water in a hydrophobic well (contact angles of 130°); right: case of water in a hydrophilic well (contact angles 50°). The "free" surface is tilted downwards or upwards depending on the contact angle. The walls have been dematerialized for clarity.

1.4 Measuring the Surface Tension of Liquids

We have remarked that surface tension can be seen as a force. Surface tension can then be measured by comparison with another known and calibrated force. This other force can be pressure as in the "bubble pressure method", also known as the Schrödinger method, or it can be a capillary force as in the Wilhelmy plate method, or it can be gravity as in the pendant drop method, and more recently it can be fluid stress as in the drop deformation method. In the following, we analyze these methods. Devices that are used to measure the surface tension are called tensiometers.

1.4.1 Using Pressure (Bubble Pressure Method)

The idea of using pressure to balance surface tension was first proposed by Erwin Schrödinger. The principle is based on the maximum pressure that an interface can support. A sketch of the experimental set up is shown in the figure 1.67. A tube filled with liquid 1 is plunged into a

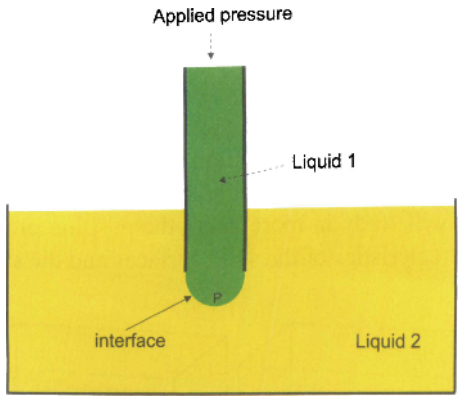

Figure 1.67 Principle of surface tension measurement using pressure: the maximum pressure which a liquid interface can support is when the interface has the shape of a half-sphere. This pressure is related to the surface tension by the Laplace law.

beaker containing liquid 2. As pressure in liquid 1 is increased, the interface at the tube outlet deforms till it reaches the form of a half-sphere. Above this maximum pressure, the interface blows out and liquid 1 breaks down into droplets flowing through liquid 2. The maximum pressure is related to the surface tension between liquid 1 and liquid 2 by the Laplace relation

$$P = 2\frac{\gamma_{L1L2}}{R_{tube}}. \tag{1.98}$$

This value can be found numerically by using the Surface Evolver (figure 1.68). We have used a capillary tube of 100 μm radius so that the gravity force does not introduce a bias in the result. Using a surface tension value of 72 mN/m (water in air), we find a maximum critical pressure of 1440 Pa, which is the value expected from (1.98). Remark: Theoretically, when the pressure is increased above the value defined by equation (1.93), the interface is no longer stable. It expands suddenly (figure 1.69) and breaks down. Physically, it corresponds to the instability of the interface and the formation of droplets. Experimentally the maximum pressure before the interface breaks is difficult to determine very precisely. This is the reason why other methods to measure surface tension have been developed.

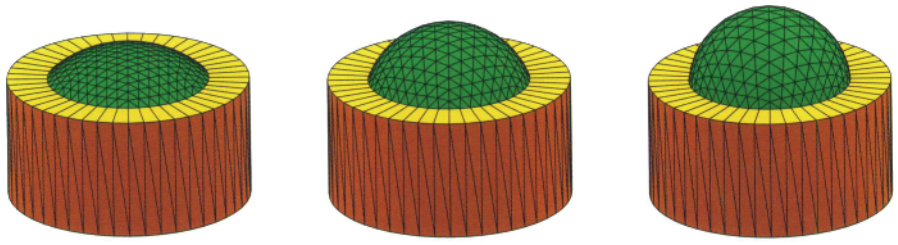

(a) P = 1000 Pa (b) P = 1350 Pa (c) P = 1440 Pa

Figure 1.68 Result of a calculation with Surface Evolver: the surface stably inflates with increasing pressures, until it reaches a half-sphere.

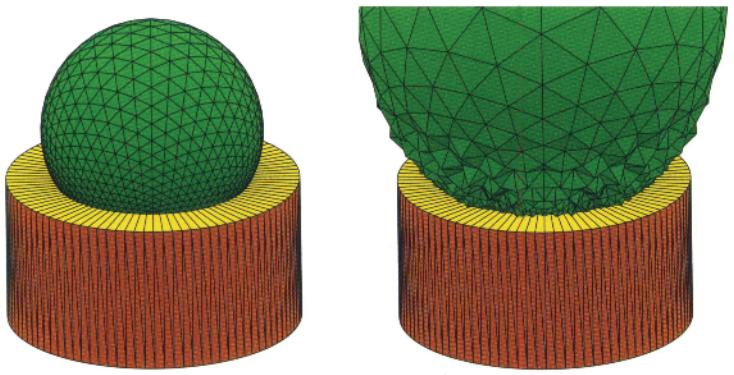

Figure 1.69 Above the threshold value the interface is no longer stable at constant pressure; it starts expanding and the numerical evolution reaches a point where the surface starts to explode.

1.4.1.1 Using the Capillary Rise on a Plate - Wilhelmy Plate

Surface tension of a liquid can be determined by measuring the capillary force exerted by the liquid on a solid plate [44]. The principle is that already described in section 1.3.7.3: the surface of the liquid rises along a vertical plate and the height reached by the liquid on the plate is proportional to the surface tension as shown by equation (1.79). In the standard method, a thin plate (perimeter about 40 mm) is lowered to the surface of a liquid and the downward force directed to the plate is measured. Surface tension is directly the force divided by the perimeter of the plate. A couple of very important points with this method must be noted. First, the plate must be completely wetted before the measurement to ensure that the contact angle between the plate and the liquid is zero. If this is not true the Wilhelmy method is not valid. Secondly, one must be sure that the position of the plate is correct, meaning that the lower end of the plate is exactly on the same level as the surface of the liquid. Otherwise the buoyancy effect must be calculated separately. Figure 1.70 shows a numerical simulation of the Wilhelmy method.

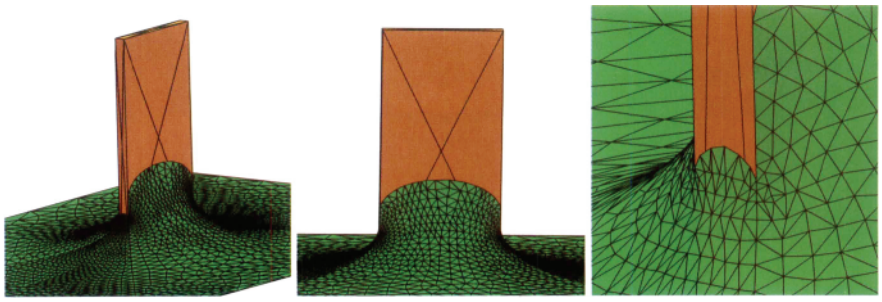

Figure 1.70 Simulation of the capillary rise along a Wilhelmy plate using the Surface Evolver: left, perspective view; middle, front view; right close-up on the contact line at a corner. Note how the contact line curves tangent to the corner in order to make a well-defined tangent plane at the corner.

1.4.2 Using Gravity: the Pendant Drop Method

By definition, a pendant drop is a drop suspended from a fixed solid, as shown in figure 1.71. The two forces acting on the drop are gravitation and surface tension. The shape of such a drop is then a function of the surface tension (figure 1.72). The pendant drop method consists of extracting the surface tension from an image of the drop shape.

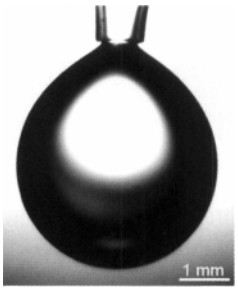

Figure 1.71 Image of a pendant drop.

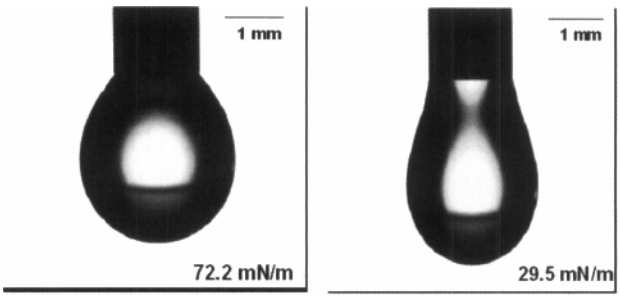

Figure 1.72 Experimental view of two drops: left: water droplet in air; right: oil droplet in air.

1.4.2.1 Bond Number

For a pendant drop, the ratio of the gravitational and surface tension forces is scaled by a non-dimensional number, the Bond number, defined by

$$Bo = \frac{\Delta\rho g R^2}{\gamma}, \tag{1.99}$$

where $\Delta\rho$ is the difference of the density of the liquid and the surrounding fluid, g the gravitational constant, γ the surface tension and R a typical dimension of the droplet. Here we choose R to be the maximum horizontal radius of the pendant drop. The shape of the pendant drop is shown in figure 1.73 for different Bond numbers. Figure 1.73 shows that, for a well chosen

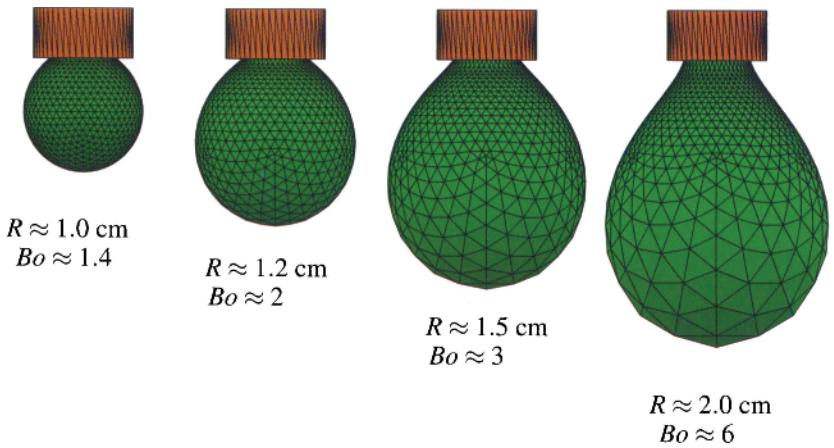

Figure 1.73 Shape of a pendant drop vs. Bond number: the drop shape departs from that of a sphere as its volume increases, until it detaches from the solid support. The liquid of the drop is water and is immersed in silicone oil; the surface tension is $\gamma = 33$ mN/m. Calculation performed with Surface Evolver.

Bond number, the competition between the gravitational force and the surface tension determines the shape of the droplet. On one hand, the gravitational force, i.e. the weight of the drop, tends to elongate the droplet vertically; on the other hand, the surface tension tends to minimize the interface by making it spherical. From an image analysis, the volume – and consequently the weight – of the drop can be determined, and also a vertical profile, which is a function of the surface tension and the weight of the drop (figure 1.74). In the following section we indicate the numerical approach that is used to determine the surface tension.

1.4.2.2 Method

There exist different numerical schemes to extract the surface tension from the pendant drop shape. A well known software is that pioneered by del Rio *et al.* called ADSA [45,46]. We do not give here the details of the method – which would be long - but just the main lines. The drop pressure is determined by writing the Laplace equation at the bottom of the droplet. Due

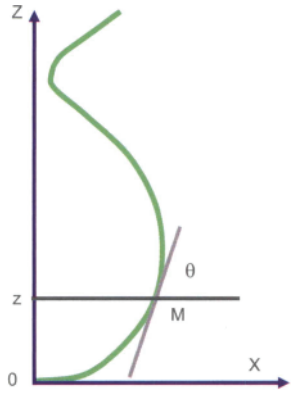

Figure 1.74 Typical drop contour in the pendant drop method.

to axisymmetry

$$\Delta P = \gamma\left(\frac{1}{R} + \frac{1}{R'}\right) = 2\frac{\gamma}{R}. \tag{1.100}$$

The curvature radius being derived from an image analysis, equation (1.100) produces the internal pressure of the drop. Second, we write the equilibrium equation of the drop in any horizontal section. Because of axisymmetry, this equilibrium imposes a zero vertical resultant:

$$2\pi R\gamma \sin\theta = V(\rho_h - \rho_l)g + \pi R^2 P. \tag{1.101}$$

In (1.101), R is the horizontal radius in the considered section, θ is the angle of the tangent at M to the contour of the image of the drop, V is the volume of the fluid under the plane of altitude z, ρ_h and ρ_l are the densities of the two fluids, and g the gravitational acceleration. The left term in equation (1.101) corresponds to the surface tension force; the first term on the right hand side, to the weight of the liquid below the considered section; and the second term on the right hand side to the pressure force. For each section, (1.101) produces a value for the surface tension γ. An averaging of all the values of γ determines precisely the real value of the surface tension.

Because the pendant drop method reacts very quickly, it is even possible to determine the surface tension as a function of the surface concentration in surfactants [47]. When CMC is reached, the shape of the drop does not evolve anymore. In conclusion, the advantages of the pendant drop method are:

- Small volume of liquid.
- Easy to spread a known amount of surfactant at the surface.
- Rapid rates of surface area change compared to Langmuir-Wilhelmy balance.

However, one must be very cautious that the capillary is very smooth and cylindrical to preserve axisymmetry.

1.4.2.3 Using Shear Stress in a Microflow

Hydrodynamic forces are usually difficult to control and to monitor accurately. However, the situation has changed drastically with the use of microflows. Such flows are completely lam-

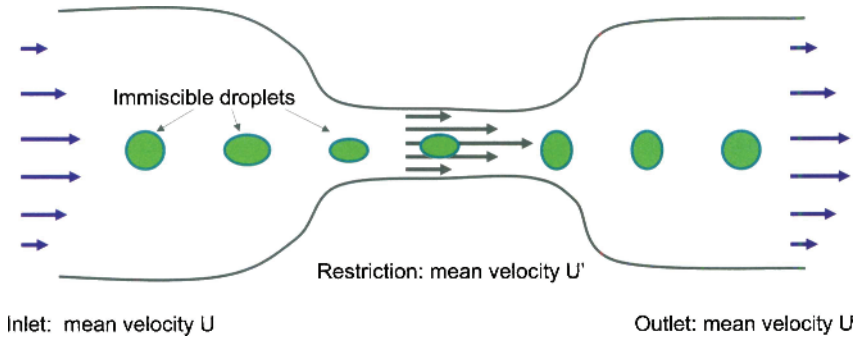

Figure 1.75 Schematic of droplet stretching in a contracted section for surface tension measurement.

inar and their velocity is largely predictable [48]. With this in mind, and observing that a droplet/bubble changes its shape according to the change in the flow mean velocity, a method for measuring surface tensions between two immiscible liquids or between a liquid and a gas has been proposed [49,50]. The principle is sketched in figure 1.75.

An experimental view of the phenomenon is shown in figure 1.76. A droplet traveling in the middle of the tube experiences a very small shear stress. However, when it reaches a constricted section, the flow accelerates and the shear stress increases. As a result the droplet takes an ellipsoidal shape oriented along the axis of the tube. At the entrance of the divergent section, the shear stress acts oppositely and the droplet takes an ellipsoidal shape oriented perpendicularly to the tube axis. After a while, the spherical shape is regained.

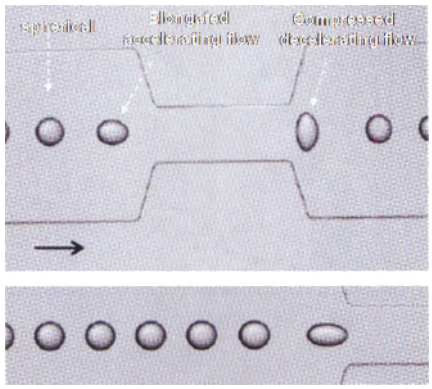

Figure 1.76 Experimental image of droplets in accelerated and decelerated fluid flows, reprinted with permission from [50], ©RSC, 2006, http://dx.doi.org/10.1039/B511976F.

Let us define the drop deformation by

$$D = \frac{a-b}{a+b}, \tag{1.102}$$

where a and b are the two vertical dimensions of the droplet. When the droplet is spherical,

$D = 0$. Let $\dot{\varepsilon}$ be the extension rate given by the change of axial velocity u,

$$\dot{\varepsilon} = \frac{du}{dx}. \tag{1.103}$$

Then it can be shown that D is given by the solution of the differential equation

$$\frac{dD}{dt^*} = \frac{5}{2\hat{\eta}+3}\tau\dot{\varepsilon} - D, \tag{1.104}$$

where t* is a nondimensional time defined by $\tau^* = t/\tau$, and $\hat{\eta} = \eta_{drop}/\eta_{carrier}$ where η denotes the dynamic viscosity. Finally τ is defined by

$$\tau = \frac{\alpha\eta_{carrier}a_0}{\gamma}, \tag{1.105}$$

where a_0 is the undistorted radius and α a rational function of $\hat{\eta}$. Instead of solving (1.105), it is convenient to re-write it in the form

$$\alpha\eta_{carrier}\left(\frac{5}{2\hat{\eta}+3}\dot{\varepsilon} - u\frac{\delta D}{\delta x}\right) = \frac{\gamma D}{a_0}. \tag{1.106}$$

D and its axial evolution $\frac{\delta D}{\delta x}$ are estimated by image analysis. Then, a plot of the quantity $\alpha\eta_{carrier}(\frac{5}{2\hat{\eta}+3}\dot{\varepsilon} - u\frac{\delta D}{\delta x})$ as a function of $\frac{D}{a_0}$ is a linear curve with slope γ. Figure 1.77 shows experimental results of the method. This microfluidic tensiometer is particularly interesting because it produces the instantaneous surface tension on line.

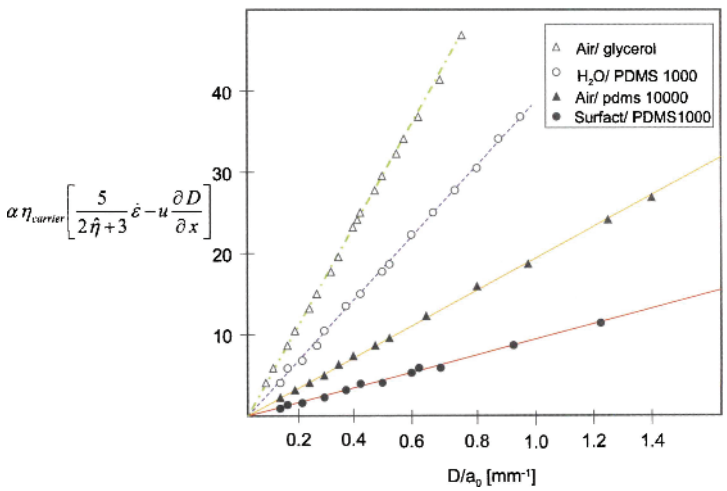

Figure 1.77 Plot of the flow extension rate versus the droplet deformation. The slope is the surface tension.

1.4.3 Surface Free Energy

1.4.3.1 Introduction

In the preceding sections, we have used the concept of surface tension of solids. However, surface tension of a solid is a complex notion; on one hand, it is very difficult to measure

intrinsically and on the other hand different analytical relation have been proposed, but their results are still not completely satisfactory [51]. In a microfluidic approach, we avoid as much as possible having to use surface tension of solids. We use Young's law as soon as it is possible to eliminate the solid surface tension, and make our approaches depend on only two values: γ_{LG} and θ. Still, we present the notion of surface free energy and in particular the notion of critical surface tension, which is important for wetting analysis.

1.4.3.2 Method of Good-Girifalco

The approach of Good and Girifalco [52] consists of expressing the work of adhesion in terms of γ_{LG} and γ_S,

$$W_a = 2\Phi(\gamma_{LG}\gamma_S)^{\frac{1}{2}}, \tag{1.107}$$

where Ψ is a function of the molar volumes of the liquid and the solid. Inserting equation (1.107) in the Young-Dupré relation (1.56) yields

$$W_a = 2\Phi(\gamma_{LG}\gamma_S)^{\frac{1}{2}} = \gamma_{LG}(1+\cos\theta), \tag{1.108}$$

leading to

$$\gamma_S = \gamma_{LG}\frac{(1+\cos\theta)^2}{4\Phi^2}. \tag{1.109}$$

The remaining problem is to estimate Φ. Kwok and Neumann [53] made a systematic study of the contact between organic fluids and low energy surfaces. They based their approach on a dependency of the type

$$\Phi = \exp(-\beta(\gamma_{LG}-\gamma_S)^2) \simeq 1-\beta(\gamma_{LG}-\gamma_S)^2, \tag{1.110}$$

where β is a constant slightly depending on the substrate. Substituting of (1.110) in (1.108) and using Young's law yields

$$\cos\theta = -1+2\sqrt{\frac{\gamma_S}{\gamma_{LG}}}\exp(-\beta(\gamma_{LG}-\gamma_S)^2). \tag{1.111}$$

For any given substrate γ_S is constant, and by using many different liquids and measuring γ_{LG} and θ, a least-square analysis leads to the values of β and γ_S. The parameter β was found to be of the order of 0.000100 to 0.000130 $(m^2/mJ)^2$ for low energy substrate such as polystyrene and polymethacrylate.

1.4.3.3 Fowkes Method

The preceding approach does not take into consideration the polar or apolar nature of the solid. The different components of the surface energy can be taken into account by writing [54]

$$\gamma_S = \gamma_S^D + \gamma_S^P, \tag{1.112}$$

where the superscripts D and P respectively stand for "diffusive" (non-polar) and polar. Neumann's approach [55] consists in subdividing the polar component into a Lewis acid and a Lewis base, so that the work of adhesion can be cast in the form

$$W_a = \gamma_{LG}(1+\cos\theta) = 2\sqrt{\gamma_{LG}^D\gamma_S^D} + 2\sqrt{\gamma_{LG}^-\gamma_S^-} + 2\sqrt{\gamma_{LG}^+\gamma_S^+}. \tag{1.113}$$

Equation (1.113) contains 8 parameters. The contact angle θ can be measured, and the properties of the liquid are also known (they can be measured). Then we are left with 3 unknowns describing the solid. If we first use a non-polar liquid ($\gamma_{LG}^{-} = \gamma_{LG}^{+} = \gamma_{LG}^{P} = 0$) then (1.113) simplifies to

$$W_a = \gamma_{LG}(1+\cos\theta) = 2\sqrt{\gamma_{LG}^{D}\gamma_{S}^{D}}, \tag{1.114}$$

and we deduce γ_S^D. More generally if we use three liquids – including a non-polar one – we find a system of three equations with the three unknowns $(\gamma_S^D, \gamma_S^+, \gamma_S^-)$. The total solid surface tension is then given by the relation

$$\gamma_S = \gamma_S^D + \gamma_S^P = \gamma_S^D + 2\sqrt{\gamma_S^+\gamma_S^-}. \tag{1.115}$$

A very instructive example has been given by Combe *et al.* for measuring the surface tension of the enamel of human teeth [56].

1.4.3.4 Critical Surface Tension and Surface Free Energy

A very general question in capillary studies is: would a given liquid completely wet a given solid or not? In other words, what is the condition for spreading? Zisman and coworkers pioneered this problem in the 1950s, with the introduction of the notion of "critical surface tension", denoted here CST for simplicity, and defined by the proposition: a solid surface cannot be completely wetted by a liquid if the value of the liquid surface tension is above the critical surface tension.

1.4.3.4.1 Zisman Plot Zisman and coworkers established an empirical connection between the cosine of the contact angle $\cos\theta$ and the liquid/air interfacial tension γ [57]. For a given low energy solid surface, they measured the contact angle θ for many different liquids. The plot of $\cos\theta$ as a function of γ approximates a straight line; it has the shape shown in figure 1.78.

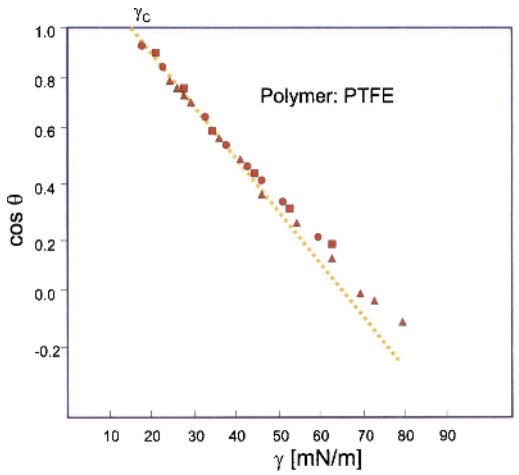

Figure 1.78 Zisman plot of the contact angle of different liquids on a PTFE surface.

When the contact angle is such that $\cos\theta = 1$, i.e. $\theta = 0$, the liquid wets the solid surface. If we denote γ_C the point where $\cos\theta = 1$, obtained by a linear extrapolation of Zisman's curves, then a liquid with a surface tension smaller than γ_C wets the surface. As a matter of fact, this nearly linear behavior is valid not only for pure liquids, but also for aqueous solutions. Zisman's approach was later refined by Bargeman *et al.* [58]. Observing that Zisman's curves were not exactly linear, especially for aqueous solutions, they have shown that linearity could be achieved by considering the relation between $\gamma\cos\theta$ and γ instead of the relation between $\cos\theta$ and γ (figure 1.79). In summary, there is a linear relation between adhesion tension and surface tension of aqueous solutions,

$$\gamma_{LG}\cos\theta = a\gamma_{LG} + b, \tag{1.116}$$

where a and b are constants depending on the solid surface.

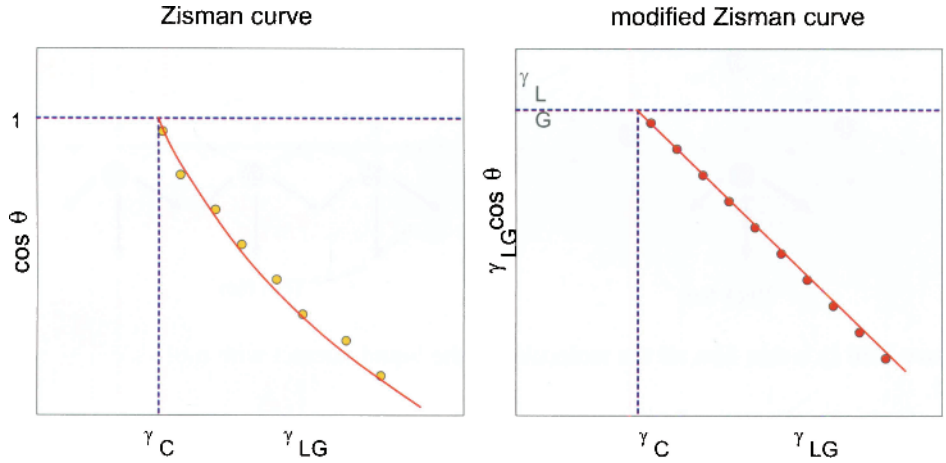

Figure 1.79 Modified Zisman's plot for PMMA (polymethyl methacrylate) and PTFE (polytetrafluoroethylene).

Zisman's approach is very practical; it easily produces the value of the CST. It has been observed that the value of the CST is often close to that of the surface tension of the solid, i.e. the Surface Free Energy (SFE). For a liquid whose surface tension approaches the critical surface tension, Young's law can be written

$$\gamma_{LG} = \gamma_C = \gamma_{SG} - \gamma_{SL}. \tag{1.117}$$

We have seen that in partial wetting conditions, there is a precursor film on the solid substrate; this is evidently the case at the onset of total wetting. This precursor film has a film pressure P_e (we discuss the film pressure in the next section) so that the surface tension γ_{SG} is given by

$$\gamma_S - P_e = \gamma_{SG}, \tag{1.118}$$

and (1.112) can be cast in the form

$$\gamma_S = \gamma_C + (\gamma_{SL} + P_e). \tag{1.119}$$

For a liquid having a surface tension γ_C, the term inside the parenthesis on the right hand side of (1.119) is often small. This is in particular the case when the solid surface is apolar, i.e. the

polar component of the surface free energy is negligible. For example PMMA has a CST of 33.1 mN/m and a SFE of 39 mN/m; PTFE has a CST of 20 mN/m and a SFE of 23.4 mN/m. In such cases the CST is a good approximation of the SFE. The advantage is that the critical surface tension can easily be obtained by Zisman plots.

1.4.3.4.2 Disjoining Pressure When a liquid film on a solid is very thin (like the precursor film), all the liquid molecules have an interaction with the solid wall, as sketched in figure 1.80. We are then at a very small scale (less than 1 nm). The energy of the film takes a special form. For a thick film, the energy is $\gamma+\gamma_{SL}$. For a thin film of thickness e the film energy is [22]

$$E = \gamma+\gamma_{SL}+P_e(e), \tag{1.120}$$

where $P_e(e)$ is a function of e such that $P_\infty = 0$ and $P_0 = \gamma_S - (\gamma+\gamma_{SL})$.

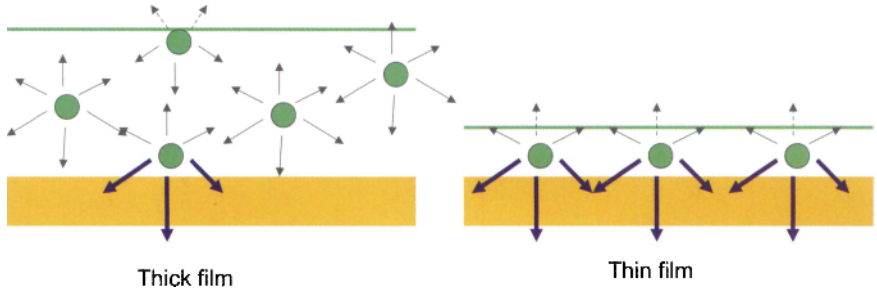

Figure 1.80 In a thin film all the molecules in the liquid interact with molecules of the solid wall.

From a thermodynamical point of view, Derjaguin has introduced the notion of "disjoining pressure" in the chemical potential [59],

$$\mu = \mu_0 + \frac{dP_e}{de}V_0 = \mu_0 - \Pi_e V_0, \tag{1.121}$$

where V_0 is the molar volume in the liquid phase. The quantity Π_e in (1.122), defined by

$$\Pi_e = -\frac{dP_e}{de}, \tag{1.122}$$

has the dimension of a pressure. Π_e is called the "disjoining pressure". With this definition, and using (1.119), de Gennes [22] shows that the total surface tension of a thin film is given by

$$\gamma_{film} = \gamma_{LG}+\gamma_{SL}+P_e+e\Pi_e. \tag{1.123}$$

We have seen that bubbles and droplets at equilibrium tend to take a spherical shape. If this were not the case, the internal pressure would not be uniform since the Laplace law applied in regions of different curvatures would produce different internal pressures. In consequence, there is liquid motion inside the bubble/droplet in order to equilibrate the internal pressure (figure 1.81).

But what about adjacent droplets or bubbles? The sketch of figure 1.81 shows that a droplet is deformed by the presence of the neighboring droplet and its curvature is not constant. A

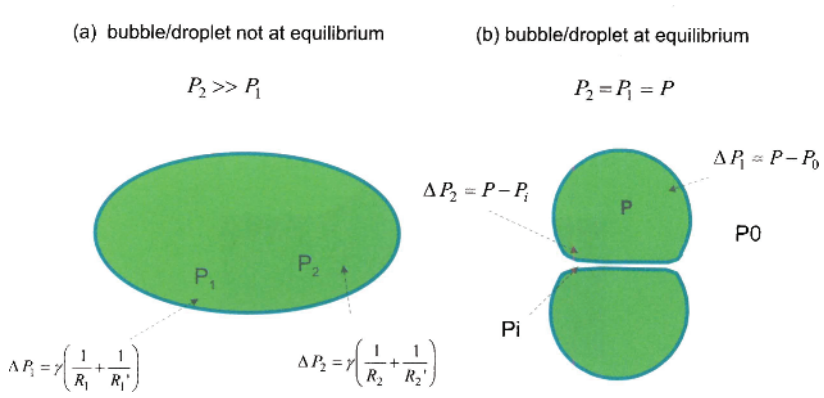

Figure 1.81 Schematic of a droplet out of equilibrium (left) and an assembly of two droplets/bubbles at equilibrium (right).

first analysis using Laplace's law would conclude that the internal pressure is not uniform. In reality, the pressure in the thin film between the drops/bubbles is not the external pressure P_0 but a different pressure related to the "disjoining pressure". According to Laplace equation, the film pressure equilibrates the pressure jump across the interface, and we have the relations

$$\Delta_{P_1} = \gamma\left(\frac{1}{R_1} + \frac{1}{R_1'}\right) = P - P_0 \Delta_{P_2} = \gamma\left(\frac{1}{R_2} + \frac{1}{R_2'}\right) = P - P_i, \tag{1.124}$$

where indices 1 and 2 refer to two locations, a first one far from the deformed interface and the other close to the deformed interface. In (1.112), P_i is the film pressure.

1.5 Minimization of the Surface Energy and Minimal Surfaces

"Minimal surfaces" are a particular type of surface. From a mathematical standpoint, a minimal surface is officially just a surface with zero mean curvature. This definition is very restrictive: there are not many minimal surfaces with known equations. One can find a description of these surfaces in reference [60]. These surfaces locally minimize their area. In the domain of physics of liquid interfaces, we have already seen an example of a minimal surface in section 1.3.3.5 with the surface of a liquid rising along a cylindrical vertical tube (figure 1.82). Another example of a minimal surface is that of the catenoid (figure 1.83). Physically, a catenoid is the surface formed by a liquid film spanning two solid rings. It is a general thermodynamic principle in physics that systems evolve to their minimal energy level. In particular, this is the case of interfaces. Surfaces of droplets in static equilibrium have a minimal free energy. Thus, in the domain of liquid interfaces, we are tempted to give a less restrictive definition for minimal surfaces. A minimal surface is a surface that minimizes its area under some constraints. The goal is to minimize the energy of the system (surface, gravitational, etc.) under some constraints imposed by external conditions, like walls, wires, fixed volume or fixed pressure. With this definition, minimal surfaces comprise a much larger set of surfaces and describe liquid films and interfaces [43,61]; when gravity is negligible, these surfaces have a constant mean curvature [62].

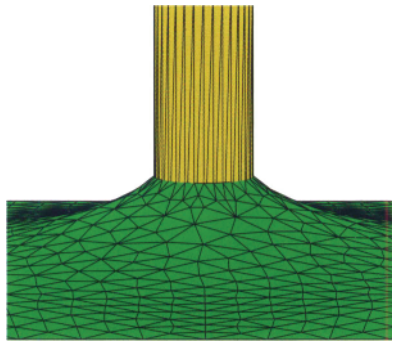

Figure 1.82 Minimal surface formed by the interface of a liquid with a vertical rod.

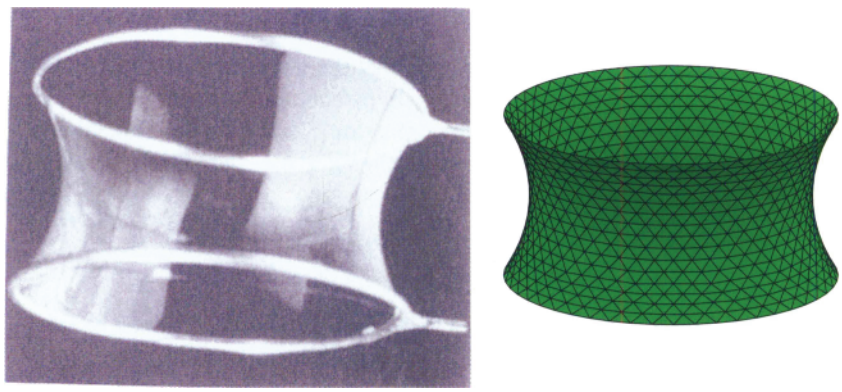

Figure 1.83 Left: Image of a soap film between two solid circles; right: result of this calculation with the Surface Evolver.

1.5.1 Minimization of the Surface Energy

According to the extended definition of a minimal surface, the droplet interface can be calculated by minimization of its surface energy. In the absence of a droplet on the surface of the solid substrate, the surface energy is

$$E_{SG,0} = \gamma_{SG} S_{SG,0}. \tag{1.125}$$

After deposition of the droplet, the surface energy is the sum of the three surface energies

$$E = E_{LG} + E_{SL} + E_{SG,1}, \tag{1.126}$$

where $E_{SG,1}$ is the surface energy of the solid surface in contact with the gas. Then, we have

$$E = E_{LG} + \int\int_{S_{SL}} (\gamma_{SL} - \gamma_{LG})\, dA + E_{SG,0}. \tag{1.127}$$

The last term on the right hand side of (1.123) does not depend on the drop shape. Thus, we have to minimize

$$E = \gamma_{LG} S_{LG} + \int\int_{S_{SL}} (\gamma_{SL} - \gamma_{LG})\, dA. \tag{1.128}$$

Taking into account Young's law, the energy to be minimized is

$$E = \gamma_{LG} S_{LG} + \gamma_{LG} \int\int_{S_{SL}} \cos\theta \, dA. \tag{1.129}$$

As we have mentioned earlier, the parameters intervening in equation (1.129) are θ and γ_{LG}. Thanks to Young's equation, we don't need the surface tension of the solid with the liquid or the gas. This is a real simplification since we have shown that θ and γ_{LG} can be measured relatively easily.

Equation (1.129) constitutes the basis for the calculation of droplet shapes that we develop in the next Chapter.

1.5.2 Conclusion

This chapter was devoted to the study of surface tensions and capillary forces. The main notions presented in this chapter are the relation between curvature and pressure expressed by Laplace's law, and the relation between the different surface tensions and contact angle at the triple line expressed by Young's law. From these two relations, an expression for the capillary force on a triple line has been deduced. Such an expression has a key role in determining the behavior of droplets on different substrates and geometry in microsystems that we shall consider in the next Chapter.

This Chapter has shown the essential role of surface tension and capillarity at the microscale. These forces often dominate forces such as gravity or inertia, which are predominant at the macroscopic scale. Although we have taken the stance of presenting capillarity and surface tension from an engineering point of view by considering global effects, one has to keep in mind that interactions at the nanoscopic scale are the real underlying causes of these global effects.

1.6 References

[1] J. Berthier, *Microdrops and digital microfluidics*. William Andrew Publishing, 2008.

[2] J. Israelachvili, *Intermolecular and surface forces*. Academic Press, 1992.

[3] Table of surface tension for chemical fluids: http://www.surface-tension.de/.

[4] G. Navascues, "Liquid surfaces: theory of surface tension," *Rep. Prog. Phys.* **42**, pp. 1133–1183, 1979.

[5] R. Eötvös, *Wied. Ann. Phys.*, **27**, pp. 445-459, 1886.

[6] E.A. Guggenheim, "The principle of corresponding states," *J. Chem. Phys.* **13**, pp. 253–261, 1945.

[7] A. Alexeev, T. Gambaryan-Roisman, P. Stephan, "Marangoni convection and heat transfer in thin liquid films on heated walls with topography: Experiments and numerical study," *Phys. Fluids* **17**(6), p. 062106, 2005.

[8] K. Szymczyk, A. Zdiennicka, B. Janczuk, W. Wocik, "The wettability of polytetrafluoroethylene and polymethyl methacrylate by aqueous solution of two cationic surfactants mixture," *J. Colloid. Interface Science* **293**, pp. 172–180, 2006.

[9] MIT, Lecture 4, Marangoni flows, http://web.mit.edu/1.63/www/Lec-notes/Surfacetension/Lecture4.pdf.

[10] F. Ravera, E. Santini, G. Loglio, M. Ferrari,L. Liggieri, "Effect of Nanoparticles on the Interfacial Properties of Liquid/Liquid and Liquid/Air Surface Layers," *J. Phys. Chem. B* **110 (39)**, pp. 19543–19551, 2006.

[11] E. Weisstein, http://mathworld.wolfram.com/Curvature.html.
[12] E. Berthier, D.J. Beebe. "Flow rate analysis of a surface tension driven passive micropump," *Lab On a Chip* **7** (11), pp.1475–1478, 2007.
[13] L.M. Pismen, B.Y. Rubinstein, I. Bazhlekov, "Spreading of a wetting film under the action of van der Waals forces," *Physics of Fluids* **12 (3)**, p. 480, 2000.
[14] P.G. deGennes, "Wetting: statistics and dynamics," *Rev. Mod. Phys.* **57**, p. 827, 1985.
[15] Quanzi Yuan, Ya-Pu Zhao, "Precursor film in dynamic wetting, Electrowetting and Electro-Elasto-Capillarity," *Phys. Rev. Let.* **104**, p.246101, 2010.
[16] C. Iwamoto, S. Tanaka, "Atomic morphology and chemical reactions of the reactive wetting front," *Acta Materiala* **50**, pp. 749, 2002.
[17] A.L. Yarin, A.G. Yazicioglu, C. M. Megaridis, "Thermal stimulation of aqueous volumes contained in carbon nanotubes: experiment and modelling," *Appl. Phys. Lett.* **86**, p.013109, 2005.
[18] Nanolane: http://www.nano-lane.com/wetting-afm.php.
[19] L. Pismen, "Dewetting patterns, moving contact lines, and dynamic diffuse interfaces," *CISM lecture notes*, Udine, Italy, 16-20 October 2006.
[20] J. Berthier, Ph. Clementz, O. Raccurt, P. Claustre, C. Peponnet, Y. Fouillet, "Computer aided design of an EWOD microdevice," *Sensors and Actuators A* **127**, pp. 283-294, 2006.
[21] K. Brakke, "The Surface Evolver," *Exp. Math.* **1**, pp. 141–165, 1992.
[22] de Gennes, P-G., F. Brochard-Wyart, D. Quèrè, *Drops, bubbles, pearls, waves.* Springer, New York, 2004.
[23] A.A. Darhuber, S.M. Troian,"Principles of microfluidic actuation by modulation of surface stresses," *Annu. Rev. Fluid Mech.* **37**, pp. 425–455, 2005.
[24] H. Bouasse, *Capillarité, phénomènes superficiels.* Delagrave, Paris, 1924.
[25] C.D. Murray,"The physiological principle of minimum work. 1. The vascular system and the cost of blood volume," *Proc. Natl. Acad. Sci. USA* **12**, pp. 207–214, 1926.
[26] L.A. Taber, S. Ng, A.M. Quesnel, J. Whatman, C.J. Carmen, "Investigating Murray's law in the chick embryo," *J. Biomech.* **34**(1), pp. 121–124, 2001.
[27] K.A. Mc Culloh, J.S. Sperry, F.R. Adler, "Water transport in plants obeys Murray's law," *Nature* **421**, pp. 939–942, 2003.
[28] E. Goljan, *Pathology*, 2nd ed., Mosby Elsevier, Rapid Review Series, 1998.
[29] H.D. Prange, "Laplace's law and the alveolus: a misconception of anatomy and a misapplication of physics," *Adv. Physiol. Educ.* **27**, pp. 34–40, 2003.
[30] J. Atencia, D.J. Beebe, "Controlled microfluidic interfaces," *Nature* **437**, pp. 648–655, 2005.
[31] T. Thorsen, R.W. Roberts, F.H. Arnold, S.R. Quake, "Dynamic pattern formation in a vesicle-generating microfluidic device," *Phys. Rev. Lett.* **86**(18), pp. 4163–4166, 2001.
[32] J. Berthier, S. Le Vot, P. Tiquet, N. David, D. Lauro, P.Y. Benhamou, F. Rivera, "Highly viscous fluids in pressure actuated Flow Focusing Devices," *Sensors and Actuators A* **158**, pp. 140–148, 2010.
[33] Y.-C. Tan, K. Hettiarachchi, M. Siu, Y.-R. Pan, A.P. Lee, "Controlled microfluidic encapsulation of cells, proteins and microbreads in lipid vesicles," *JACS* **128**(17), pp. 5656-5658, 2006.
[34] L. Landau, E. Lifchitz, *Fluid mechanics*, 2nd edition: Volume 6, Reed Educational and Professional Publishing, Oxford, 2000.
[35] Y.S. Yu, Y.P. Zhao, "Deformation of PDMS membrane and microcantilever by a water droplet: Comparison between Mooney-Rivlin and linear elastic constitutive models,"

Journal of Colloid and Interface Science **332**, pp. 467–476, 2009.

[36] X.H. Zhang, X.D. Zhang, S.T.Lou, Z.X. Zhang, J.L.Sun, J. Hu, "Degassing and temperature effects on the formation of nanobubbles at the mica/water interface," *Langmuir* **20**(9), pp. 3813–3815, 2004.

[37] J.Y. Wang, S. Betelu, B.M. Law, "Line tension approaching a first-order wetting transition: Experimental results from contact angle measurements," *Physical Review E* **63**, pp. 031601-1, 031601-10, 2001.

[38] J. Drehlich, "The significance and magnitude of the line tension in three-phase (solid-liquid-fluid) systems," *Colloids and Surfaces A: Physicochemical and Engineering Aspects* **116**, pp. 43–54, 1996.

[39] D.L. Hu, J. W. M. Bush, "Meniscus-climbing insects," *Nature* **437**, pp. 733–736, 2005.

[40] J. Jurin, "An account of some experiments shown before the Royal Society; with an enquiry into the cause of the ascent and suspension of water in capillary tubes," *Philosophical Transactions of the Royal Society* **30**, pp.739–747, 1719.

[41] Y. Tsori, "Discontinuous liquid rise in capillaries with varying cross-sections," *Langmuir* **22**, pp. 8860–8863, 2006.

[42] Jun Zeng, T. Korsmeyer, "Principles of droplet electrohydrodynamics for lab-on-a-chip," *Lab Chip* **4**, pp. 265–277, 2004.

[43] J. Berthier, Ph. Dubois, Ph. Clementz, P. Claustre, C. Peponnet, Y. Fouillet, "Actuation potentials and capillary forces in electrowetting based microsystems," *Sensors and Actuators, A: Physical* **134**(2), pp. 471-479,2007.

[44] K. Holmberg, *Handbook of Applied Surface and Colloid Chemistry.* New York, Wiley and Sons, 2002.

[45] O.I. del Rio, A.W. Neumann,"Axisymmetric drop shape analysis: computational methods for the measurement of interfacial properties from the shape and dimensions of pendant and sessile drops," *J. Coll. Int. Sci.* **196**, pp. 134–147, 1997.

[46] M. Hoofar, A.W. Neumann, "Axisymmetric drop shape analysis (ADSA) for the determination of the surface tension and contact angle," *J. Adhesion* **80**(8), pp. 727–743, 2004.

[47] H.A. Wege, J.A. Holgado-Terriza, M.J. Galvez-Ruiz, M.A. Cabrerizo-Vilchez, "Development of a new Langmuir-type pendant drop film balance," *Colloids and Surfaces B: Biointerfaces* **12**, pp 339–349, 1999.

[48] J. Berthier, P. Silberzan, *Microfluidics for Biotechnology.* Artech House, 2005.

[49] S.D. Hudson, J.T. Cabral, W.J. Goodrum, Jr., K.L. Beers, E.J. Amis, "Microfluidic interfacial tensiometry," *Applied Physics Letters* **87**, p. 081905, 2005.

[50] J.T. Cabral, S.D. Hudson, "Microfluidic approach for rapid multicomponent interfacial tensiometry," *Lab Chip* **6**, pp. 427–436, 2006.

[51] L. Makkonen,"On the methods to determine surface energies," *Langmuir* **16**, pp. 7669–7672, 2000.

[52] R.J. Good, L.A. Girifalco,"A theory for estimation of surface and interfacial energies. 3. Estimation of surface energies of solids from contact angle data," *J. Phys. Chem.* **64**, pp. 561–565, 1960.

[53] D.Y. Kwok, A.W. Neumann,"Contact angle interpretation in terms of solid surface tension," *Colloids and Surfaces A: Physicochemical and Engineering Aspects* **161**(15), pp. 31–48, 2000.

[54] F.M. Fowkes, "Additivity of intermolecular forces at interfaces. 1. Determination of contribution to surface and interfacial tensions of dispersion forces in various liquids," *J. Phys. Chem.* **67**(12), p. 2538, 1963.

[55] A.W. Neumann, R.J. Good, C.J. Hope, M. Seipal, "Equation of state to determine surface

tensions of low energy solids from contact angles," *J. Colloid Interf. Sci.* **49**, pp. 291–304, 1974.

[56] E.C. Combe, B. A. Owen, J.S. Hodges,"A protocol for determining the surface energy of dental materials," *Dental Materials* **20**, pp. 262–268, 2004.

[57] W.A. Zisman, "Contact angle, wettability and adhesion," *Advances in Chemistry Series* **43**, p. 1, 1964.

[58] D. Bargeman, F. van Voorst Vader, "Tensile strength of water," *J. Coll. Sci.* **42**, pp. 467–472, 1973.

[59] A. Adamson, A. Gast, *Physical Chemistry of Surfaces*, 6th edition. John Wiley and Sons Inc., 1997.

[60] Brandeis University: http://rsp.math.brandeis.edu/3D-XplorMath/Surface/gallery_m.html.

[61] K. Brakke, "Minimal Surfaces, Corners, and Wires," *J. Geom. Anal.* **2**(1), pp. 11–36, 1992.

[62] D.E. Hewgill, "Computing surfaces of constant mean curvature with singularities," *Computing* **32**, pp. 81–92, 1984.